REPORT R-591 OCTOBER, 1972 UILU-ENG 72-2253

CSL COORDINATED SCIENCE LABORATORY

SYNTHETIC HOLOGRAMS AND IMAGE RECONSTRUCTION FROM ACOUSTIC OR MICROWAVE FIELD PATTERNS

THEMISTOCLES H. DEMETRAKOPOULOS
RAJ MITTRA

UNIVERSITY OF ILLINOIS - URBANA, ILLINOIS

UILU-ENG 72-2253

SYNTHETIC HOLOGRAMS AND IMAGE RECONSTRUCTION FROM ACOUSTIC OR MICROWAVE FIELD PATTERNS

by

Themistocles H. Demetrakopoulos

and

Raj Mittra

This work was supported in part by the Joint Services Electronics Program (U. S. Army, U. S. Navy and U. S. Air Force) under Contract DAAB-07-67-C-0199, and in part by the Army Research Office under Army Research Grant G-77.

ABSTRACT

Recently there has been much interest in the area of acoustic or microwave holography since the use of these sources allow one to image through some optically opaque media.

Optical reconstruction applied to holograms that have been recorded at microwave, acoustic or other sub-optical frequencies produces a longitudinally distorted image, unless the original hologram has been reduced by the ratio of the recording to reconstructing wavelength. Since the required reduction ratio is very large it is difficult to achieve it in practice. Also, a hologram reduced in this manner reproduces an image that is extremely small. In this investigation a technique is presented for the reduction, or complete elimination, of the longitudinal distortion in three-dimensional imaging from synthetic holograms. The object is longitudinally demagnified in the recording process, an optical hologram is synthesized and subsequently reduced by a suitable factor. Next, the image is reconstructed by illuminating the hologram with laser light. Due to the difference of the recording and reconstructing wavelengths the image is longitudinally distorted. However, in principle the longitudinal demagnification introduced in the recording process can be made to compensate, either totally or in part, the longitudinal magnification introduced in the reconstruction process. In practice the large depth of focus inherent from the small ratio of the hologram aperture to wavelength limits the use of this technique to partial compensation only.

In addition to the optical reconstruction technique described above digital reconstruction has also been applied to simulated acoustic

or microwave diffraction patterns. In this method the transverse cross-sections of three-dimensional objects are evaluated and sequentially displayed on a CRT. Information about the three-dimensional nature of an object can be gained from these displays.

Both the optical and digital techniques have certain advantages and disadvantages; however, depending upon a specific application one may be used to supplement the other in three-dimensional image reconstruction.

TABLE OF CONTENTS

LIST OF FIGURES

LIST OF FIGURES (continued)

1. INTRODUCTION

Optical holography, the method of recording and reconstructing the amplitude and phase distribution of a wavefront was first invented by Dennis Gabor in 1949 (Gabor, 1949,1951). Leith and Upatnieks, having at their disposal a newly discovered coherent light source, the laser, modified and improved Gabor's method; and construction of three-dimensional images of three-dimensional objects became possible (Leith and Upatnieks, 1962,1963, 1964).

Shortly after optical holography was recognized as a technique for making three-dimensional images, many researchers have been successful in applying the physical principles of optical holography to what now is called acoustical and microwave holography. Acoustical holography enables one to form images of objects which are located inside media that are opaque to light waves. When fully developed it could be of great benefit to many areas such as medicine, geology, oceanography and structural engineering (Korpel, 1968, Feleppa, 1972). Microwave holography can be used to form images of objects without the presence of light (Kock, 1969).

Simultaneously with advances in holography and computer technology, computer generated holograms came into being. Several different methods for synthesizing holograms have been introduced in recent years (Waters, 1966, Kozma and Kelley, 1965, Lesem, Hirsch, Jordan, 1967, Lohmann and Paris, 1967, Lesem et al., 1969, Lee, 1970). Synthetic holograms further increase the domain of holography. They find applications in areas of optics where an optical wavefront needs to be generated or modified. Synthetic holograms

can be used in three-dimensional displaying (Lesem et al., 1968), optical spatial filtering (Vander Lugt, 1968, Lohmann and Paris, 1968), testing of optical surfaces (MacGovern and Wyant, 1971, Ichioka et al., 1971) and reconstruction of images from acoustic and microwave holograms (Goodman, 1969). The review article on Digital Holography by Huang (1972) examines the various methods of synthesizing holograms and their uses. Moreover it gives many related references.

Using holographic principles in imaging techniques, the use of lenses is eliminated and thus no problem arises concerning the state of the art of acoustic and microwave lenses. Also eliminated is the possible problem of locating a lens inside a medium. However, no recording medium has been invented that will directly record interference patterns at acoustic or microwave frequencies as photographic film records interference patterns at optical frequencies; thus, we have to rely upon sampling techniques in the recording process. Note that although these techniques have the disadvantage of being slow, nevertheless, they do provide a viable alternative to photographic recording. The method of direct sampling of the interference pattern becomes more attractive due to the fact that the reference wave does not have to be superimposed on the object wave, but it can be supplied electronically (Deschamps, 1967).

Typically, in order to reconstruct optical images of objects from non-optical holograms, such as microwaves, acoustic or computer generated holograms, the hologram is sampled using a probe and the intensity is displayed on a CRT. Then a transparency of the recorded interference pattern is made and scaled down optically. The hologram

can also be scaled down electronically before it is displayed on the CRT. Subsequently, using a laser as a coherent light source, the three-dimensional image of the original object is constructed (Metherell et al., 1967, Mueller, 1971).

This procedure has some disadvantages, which have been pointed out by various authors (Mueller et al., 1969). The scaling factor $\frac{1}{\mu}$ is given by the relation

$$\mu = \frac{\lambda_2}{\lambda_1}$$

where λ_1 is the recording wavelength and λ_2 is the reconstructing wavelength. The scaling factor $\frac{1}{\mu}$ is, in most cases, very large and difficult to achieve. If the original hologram is not scaled down exactly by the factor $\frac{1}{\mu}$, the image is longitudinally distorted (Meier, 1965). However, even if perfect scaling takes place, the final image will be very small, thus of questionable value.

If the recording is done using sampling techniques at frequencies which allow the detector to record not only the magnitude but also the phase of the scattered field, then a reference wave is not needed. There is enough information in the recorded scattered field for the three-dimensional reconstruction of the object.

In this report we suggest a method for alleviating the problem of longitudinal distortion (depth magnification) in the image of a three-dimensional object derived from a computer generated hologram. The principle of the method is as follows. Using digital techniques the object to be imaged is longitudinally demagnified in the recording process.

Subsequently in the reconstruction process longitudinal magnification occurs due to the difference between the recording and reconstructing wavelengths. Thus these two effects may be made to cancel each other so that the final image is free of distortion. In addition to this technique we also suggest a method for digital reconstruction of an image from sound or microwave diffraction patterns. Similar techniques have previously been applied to the imaging of two-dimensional objects (Sondhi, 1969, Boyer et al., 1971, Aoki, 1970). In this work we extend the method to apply to three dimensional objects as well. It should be realized, of course, that using this method the entire three-dimensional image of the object is not displayed simultaneously; rather various cross sections of the object are displayed in a sequential fashion to exhibit the depth information. One of the advantages of using digital reconstruction is that the image size thus obtained is considerably larger than that possible by optical reconstruction. Digital reconstruction also has the advantage of eliminating photographic processing. Thus it is possible, using this method, to achieve an almost real time display of the object.

The investigation reported in the following pages has been separated into two main parts: a) correction of the longitudinal distortion of objects in computer generated holograms, b) the digital construction of three dimensional objects from their sound or microwave diffraction field patterns.

In Chapter 2 an analysis of the lateral and longitudinal magnifications is given for a general case of construction and reconstruction of holograms. Then the technique of reducing the longitudinal distortion

is introduced and discussed. In Chapter 3 the forward diffraction pattern for a three-dimensional object is evaluated and a synthetic hologram is made. The optical reconstruction is applied and experimental results are given in Chapter 4.

In Chapter 5, digital reconstruction is applied to simulated microwave or acoustic holograms. The reconstructed cross sections of the object are displayed on a cathode ray tube and pictures of these patterns are shown. Finally, in Chapter 6, a general discussion of the methods and results is given.

2. THEORY OF THE RECORDING OF HOLOGRAMS AND RECONSTRUCTION OF IMAGES

2.1. Recording of Holograms

Before we embark upon the application of the technique of reducing the longitudinal distortion of the images occurring in holograms in which the recording and reconstruction wavelengths differ, we examine the basic principles of the recording of holograms and construction of images from a general view point. The same principles will be carried over to the computer generated holograms. The literature is very extensive (Smith, 1969, Stroke, 1969, DeVelis and Reynolds, 1967, Collier et al., 1971).

Figure 2.1 shows the basic arrangement for the construction of a hologram. The two mutually coherent wavefronts, the object and reference wavefronts impinge upon a detection medium forming an interference pattern. Let the recorded interference pattern, called the hologram, have the coordinates x_1', y_1', z_1' and let the recording wavelength be λ_o. The detection medium can be a photographic emulsion, a two dimensional array of detectors, or some other appropriate device, depending upon the type of the recording wave. The reference wave is a spherical wave originating from x_r, y_r, z_r, and has a complex amplitude $U_r(x_1', y_1', z_1')$ at the recording medium. The object wave having a complex amplitude at the recording medium of $U_o(x_1', y_1', z_1')$, is the wave transmitted or reflected from the object being located around the origin or a coordinate system x_o, y_o, z_o. The recorded intensity distribution at the hologram plane is

$$I = |U_r + U_o|^2 = |U_r|^2 + |U_o|^2 + U_o^* U_r + U_o U_r^*. \qquad (2.1)$$

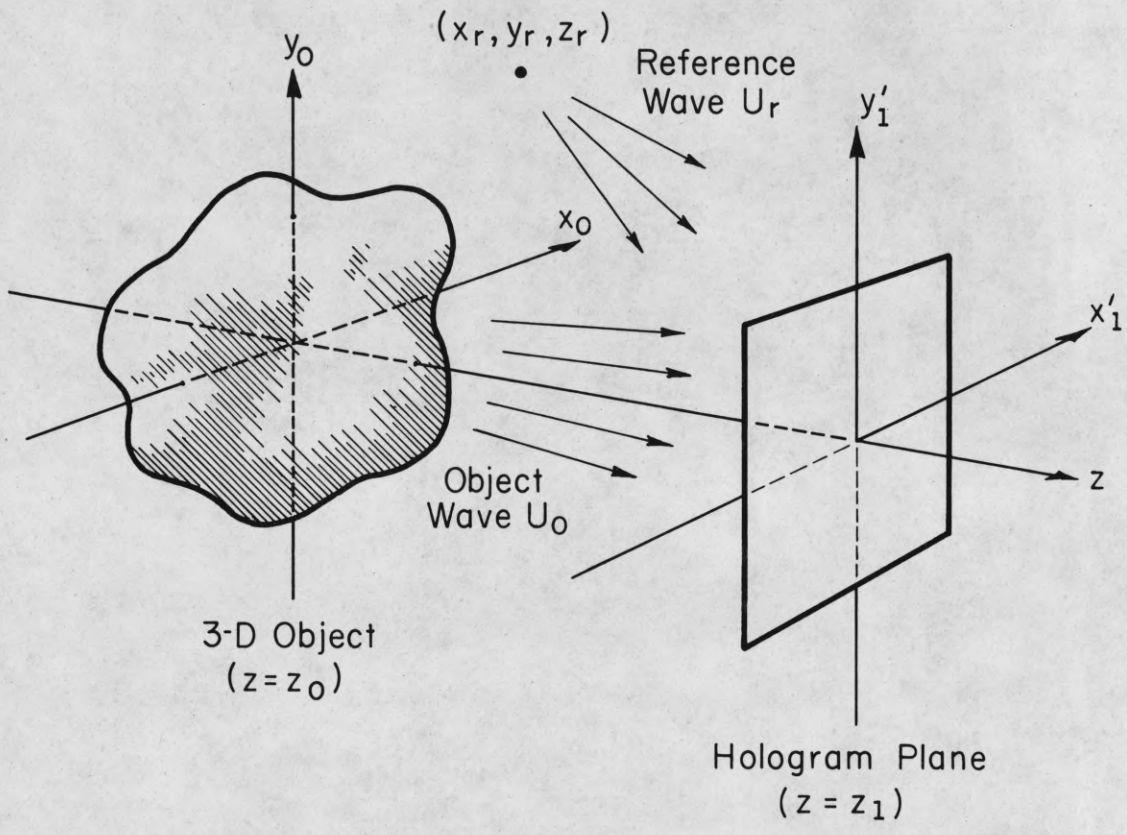

Figure 2.1 Basic Geometrical Arrangement for the Recording of a Hologram

From this recorded intensity we want to recover the object wavefront U_o.

If the recording wave is an optical one, photographic film or other photosensitive material is used to record the intensity I. Then the film is processed, and the developed photographic transparency is used in the reconstruction. If the recording wave is a microwave or sound wave, the intensity I is sampled, and if an optical reconstruction of U_o is desired, the intensity of the sampled points is plotted on a photosensitive film for further processing and construction of a transparency.

2.2. Construction of Images

Before reconstruction is applied, the hologram may be reduced or enlarged by a factor m: thus we have a transformation of the coordinates x_1', y_1' to x_1, y_1 by the relation,

$$x_1 = mx_1'$$

$$y_1 = my_1'$$

where x_1, y_1 are the coordinates of the reduced or enlarged hologram from which the final image will be reconstructed. Figure 2.2 shows the general geometrical arrangement for the reconstruction of images. The hologram is illuminated by a coherent spherical wavefront U_c, originating from a point of coordinates x_c, y_c, z_c. Let μ be the wavelength ratio

$$\mu = \frac{\lambda_c}{\lambda_o} \tag{2.2}$$

where λ_o, λ_c are the recording and reconstruction wavelengths respectively.

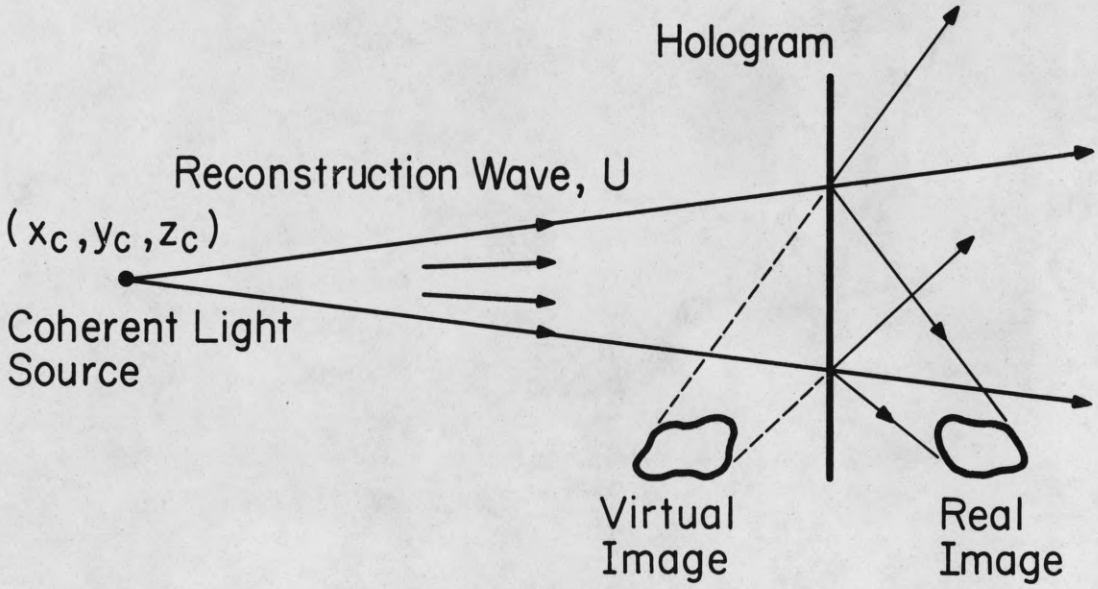

Figure 2.2 Reconstruction of Images

The emerging wavefront from the hologram transparency is

$$U = U_c I = U_c|U_r|^2 + U_c|U_o|^2 + U_c U_o^* U_r + U_c U_o U_r^* . \quad (2.3)$$

If the reference wave is equal to the reconstruction wave, i.e. $U_c = U_r$, and of constant intensity, (2.3) becomes

$$U = U_r|U_r|^2 + U_r|U_o|^2 + U_r^2 U_o^* + |U_r|^2 U_o . \quad (2.4)$$

The last term in (2.4) clearly points out that U_o is the desired object wavefront. Leith and Upatnieks (1964) by using an "off-axis" reference wave

$$U_r = Ae^{-jk\sin\theta y} \quad (2.5)$$

(where A is a constant, θ is the angle between the propagation vector k and the normal to the hologram) succeeded in spatially separating the last two terms from the first two terms in (2.4) as shown in Figure 2.2. In such a case the emerging wavefront from the hologram transparency is

$$U = A^3 e^{-jk \sin \theta y} + A|U_o|^2 e^{-jk \sin \theta y} + A^2 e^{-j2k \sin \theta y} U_o^* + A^2 U_o . \quad (2.6)$$

It can be seen from (2.6) that each term will propagate in different directions and that the last term is a replica of the original object wavefront. The third and fourth terms in (2.6) represent the real and virtual images of the object respectively. In cases where the recording and reconstructing wavelengths differ, the object and its image differ as discussed in the following section.

2.3. Magnification of Images

A rigorous analysis of the magnification and third order aberrations in holography has been given by R. Meier (1965). It has been shown in this paper that by using the general approach described above, the lateral magnification of the object is given by

$$M_{lat} = \left|\frac{\partial x_i}{\partial x_o}\right| = \left|\frac{\partial y_i}{\partial y_o}\right| = \frac{m}{1 \pm \frac{m^2}{\mu}\frac{z_o}{z_c} - \frac{z_o}{z_r}} \quad . \tag{2.7}$$

The longitudinal magnification is

$$M_{long} = \left|\frac{\partial z_i}{\partial z_o}\right| = \frac{m^2}{\mu} \frac{1}{\left[1 \pm \frac{z_o m^2}{\mu z_c} - \frac{z_o}{z_r}\right]^2} \tag{2.8}$$

The upper and lower signs in (2.7), (2.8) correspond to the virtual and real images respectively. Also x_i, y_i are the lateral coordinates and z_i is the longitudinal coordinate of the images given by:

$$x_i = \frac{m^2 x_c z_o z_r \pm \mu m x_o z_c z_r \pm \mu m x_r z_c z_o}{m^2 z_o z_r \pm \mu z_c z_r \mp \mu z_c z_o} \tag{2.9a}$$

$$y_i = \frac{m^2 y_c z_o z_r \pm \mu m y_o z_c z_r \pm \mu m y_r z_c z_o}{m^2 z_o z_r \pm \mu z_c z_r \mp \mu z_c z_o} \tag{2.9b}$$

$$z_i = \frac{m^2 z_c z_o z_r}{m^2 z_o z_r \pm \mu z_c z_r \mp \mu z_c z_o} \tag{2.9c}$$

Again the upper and lower signs in (2.9 a,b,c) correspond to the virtual and real images respectively. The rest of the terms in (2.7), (2.8), (2.9) have been defined in Sections 2.1, 2.2.

The lateral or longitudinal magnifications are the ratios of the lateral or longitudinal dimensions of the original object to the lateral or longitudinal dimensions of the image. In our case, the x,y coordinates represent the lateral dimensions and the z coordinate represents the longitudinal dimension. As it can be seen from (2.7), (2.8) the size of the reconstructed image relative to the original object depends upon the wavelength ratio μ, the magnification ratio m, and geometrical arrangement of object, reference and reconstruction waves.

From (2.7) and (2.8) we have

$$M_{long} = \frac{1}{\mu} M_{lat}^2 \tag{2.10}$$

In the case where the reference and reconstruction waves are plane waves, i.e. $z_c = z_r = \infty$ (2.7) and (2.8) become

$$M_{lat} = m \tag{2.11}$$

$$M_{long} = \frac{m^2}{\mu} = \frac{m}{\mu} M_{lat} \, . \tag{2.12}$$

Equation (2.12) shows that in the case of the reference and reconstructing waves being plane waves, the size of the reconstructed image relative to the original object depends only upon the magnification ratio and wavelength ratio.

2.4. Distortion of Images

In order for the reconstructed image to be undistorted the lateral and longitudinal magnifications must be equal. In such a case we have

$$M_{long} = M_{lat} = \frac{m^2}{\mu} = m. \tag{2.13}$$

Equation (2.13) is satisfied if $m = \mu$ which means that in order to have a completely realistic three dimensional image, the reduction of the recorded hologram must be equal to the wavelength ratio. In most cases μ is of the order of $\frac{1}{3000}$, $\frac{1}{4000}$. This indicates that a reduction ratio of ~3000, 4000 must be applied to the recorded hologram for the final image to be undistorted. With today's equipment such reductions can not be realized without introducing distortions. But even if a reduction equal to that of $\frac{1}{\mu}$ is realized, the reconstructed image will be very small and of questionable value. A microscope has to be used for enlargement, but in such a case unequal magnification is introduced and the three-dimensional aspect of the image is lost.

Another problem that arises when the original hologram is not reduced by the proper ratio, is that the distance from the hologram to the virtual or real image is very long. It is given by

$$z_i = \frac{m^2 z_c z_o z_r}{m^2 z_o z_r \pm \mu z_c z_r \mp \mu z_c z_o} =$$

$$= \frac{1}{\frac{1}{z_c} \pm \frac{\mu}{m^2 z_o} \mp \frac{\mu}{m^2 z_r}} = \left(\frac{1}{z_c} \pm \frac{\mu}{m^2 z_o} \mp \frac{\mu}{m^2 z_r}\right)^{-1} \tag{2.14}$$

where the upper sign and the lower sign correspond to the virtual and real images respectively.

For plane wave illumination in the recording and reconstruction process, $z_c = z_r = \infty$, we have

$$z_i = \pm \frac{m^2}{\mu} z_o \ . \tag{2.15}$$

Again if $m \gg \mu$, i.e. $\frac{m^2}{\mu} \gg 1$ it shows that the image will be very far from the hologram. The three dimensional aspect of the virtual image is lost due to its being very far and very small. Also, the angular magnification which is given by

$$M_{ang} = \frac{\mu}{m} \tag{2.16}$$

is very small and this means that there will be low angular separation between the noise part of the wavefront and the image. Meier (1965) in his analysis reports that third order aberrations also exist if the hologram is not scaled properly.

After pointing out the longitudinal distortion of the images and the problems of eliminating it, we next suggest a method for alleviating the problems pointed out in this section.

2.5. Modification of the Recording Process for Alleviating the Longitudinal Distortion Problem

A technique to alleviate the high reduction factor $\frac{1}{\mu}$ and thus avoid the longitudinal distortion of the image will now be suggested for computer generated holograms. In this method the coordinate z_o is reduced by a factor

m' in the recording process. More explicitly, instead of using $z = z_o$ we used $z = m'z_o$. This has the effect of contracting the object in the z direction and simultaneously bringing it closer to the recording plane.

The reduction of z by $\frac{1}{m'}$ has the effect of increasing the spatial frequencies at the hologram plane. Therefore the sampling rate must be increased to guarantee the proper sampling of the intensity function. To show how the contraction of the z dimension affects the magnification formulas we substitute $m'z_o$ for z_o in (2.7) and (2.8). Thus we have

$$M_{lat} = \frac{m}{1 \pm \frac{m^2 m' z_o}{\mu z_c} - \frac{m' z_o}{z_r}} \tag{2.17}$$

$$M_{long} = \frac{m^2 m'}{\mu} \left\{ \frac{1}{\left[1 \pm \frac{m^2 m' z_o}{\mu z_c} - \frac{m' z_o}{z_r}\right]^2} \right\} \tag{2.18}$$

For plane wave illumination from (2.17), (2.18) we obtain

$$M_{long} = \frac{m'}{\mu} M_{lat}^2 = \frac{m' m^2}{\mu} . \tag{2.19}$$

Again, for an indistorted image $M_{long} = M_{lat}$ and (2.19) gives

$$\mu = m'm. \tag{2.20}$$

It can be seen from equations (2.13) and (2.20) that $\frac{1}{\mu}$ (proper reduction ratio) in (2.20) is not as large as in (2.13). Using the technique described

above we succeed in reducing the factor $\frac{1}{\mu}$ to $\frac{1}{m'm}$ instead of $\frac{1}{m}$. It all indicates that the more we contract the z coordinate (the larger the m') in the recording process the less we have to reduce the hologram optically or otherwise. Also the final hologram to image distance z_i will not be as long as if there were no shrinking of the z axis. It will be

$$z_i = \pm \frac{m^2 m'}{\mu} z_o \tag{2.21}$$

which indicates that z_i in (2.21) is smaller than z_i in (2.15) ($m' < 1$). The reduction factor $\frac{1}{m'}$ can not be very large because this physically means that the object will be brought very close to the hologram plane, the sampling period will be very small, and more sampling points will have to be taken; computer capacity puts a limit to the number of points. Moreover the various diffraction orders of the image will not be separated. Thus we scale the z dimension down to an acceptable level and then contract the object only. In such a case a non-longitudinally distorted image results. Experimental results are given in Chapter 3.

3. CONSTRUCTION OF THE FORWARD DIFFRACTION PATTERN AND SIMULATION

3.1. Construction of the Forward Diffraction Pattern

3.1.1. Formulation of Diffraction

Consider a plane monochromatic wave of unit amplitude propagating along the z axis and illuminating an aperture of amplitude transmittance $f_o(r_o)$ where $r_o = (x_o, y_o, z_o)$. The field distribution f(r) in the half space $z > z_o$ obeys the Helmholz equation

$$(\nabla^2 + k^2) f(r) = 0 \tag{3.1}$$

where k is the wave vector, r = (x,y,z). It is assumed that f(r) obeys the Sommerfeld radiation condition at infinity

$$r\left(\frac{\partial f(r)}{\partial n} - jkf(r)\right) \to 0 \text{ as } r \to \infty \tag{3.2}$$

where $\hat{n}$ is a unit vector perpendicular to the aperture. Knowing the amplitude transmittance $f_o(r_o)$ at $(z = z_o)$ the field distribution on a plane $z = z_1 > z_o$ can be evaluated. The geometry for the construction of the forward diffraction pattern is shown in Figure 3.1. The Rayleigh-Sommerfeld scalar theory of diffraction is used to evaluate the forward diffraction pattern $f_1(r_1)$ (Mittra and Ransom, 1967, Born and Wolf, 1970, Goodman, 1968). That gives

$$f_1(x_1, y_1, z_1) = \iint_{S_o} f_o(x_o, y_o, z_o) h(x_1 - x_o, y_1 - y_o, z_1 - z_o) dS_o \tag{3.3}$$

where $h(x_1 - x_o, y_1 - y_o, z_1 - z_o)$ is called the propagation function and it is

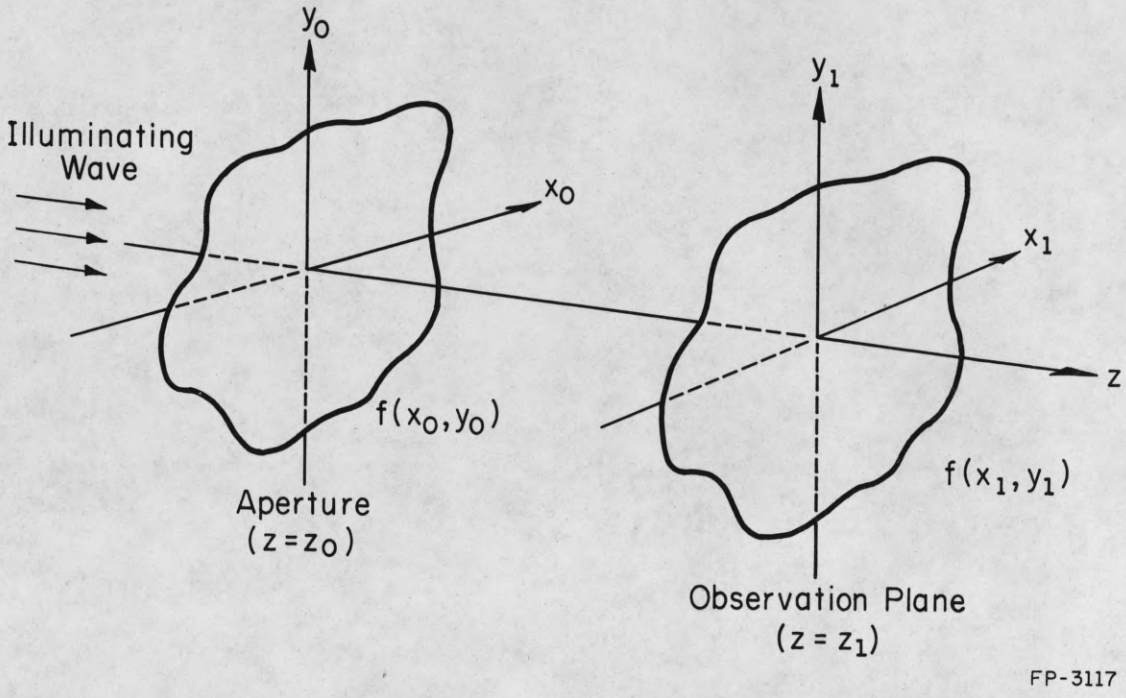

Figure 3.1 Geometry for the Evaluation of the Forward Diffraction Pattern

given by

$$h(x_1-x_o,y_1-y_o,x_1,z_1-z_o) = \frac{e^{jk|r_1-r_o|}}{j\lambda|r_1-r_o|} \cos(\bar{n},\bar{r}_{10}) \tag{3.4}$$

$$|r_{10}| = |r_1-r_o| = [(x_1-x_o)^2 + (y_1-y_o)^2 + (z_1-z_o)^2]^{\frac{1}{2}} \tag{3.5}$$

The vector $\hat{n}$ is a unit vector pointing in the -z direction, and (x_o,y_o), (x_1,y_1) are the coordinates of the aperture (object) and diffraction pattern distributions respectively. The integral in Eq. (3.3) is evaluated over the aperture S_o on the plane $z = z_o$.

For cases where the object is such that only a small area about the z axis is of interest, i.e., the distance between object and diffraction plane is very much greater than the maximum linear dimension of the object, we have the approximation

$$\cos(n,r_{10}) \simeq 1 \tag{3.6}$$

Using the same argument we can set the denominator of the propagation function in Eq. (3.4) equal to z_1-z_o, i.e., $|r_1-r_o| \simeq z_1-z_o$. Thus Eq. (3.4) becomes

$$h(x_1-x_o,y_1-y_o,z_1-z_o) \simeq \frac{e^{jk|r_1-r_o|}}{j\lambda(z_1-z_o)} \tag{3.7}$$

Fresnel's approximation can be applied to Eq. (3.7) to further simplify the exponent (Goodman, 1968). If

$$(z_1-z_o)^3 \gg \frac{\pi}{4\lambda}\left[(x_1-x_o)^2 + (y_1-y_o)^2\right]^2 \tag{3.8}$$

is satisfied, then using the approximation

$$|r_1-r_o| \simeq (z_1-z_o)\left\{1 + \frac{1}{2}\left[\left(\frac{x_1-x_o}{z_1-z_o}\right)^2 + \left(\frac{y_1-y_o}{z_1-z_o}\right)^2\right]\right\} \tag{3.9}$$

Eq. (3.7) becomes

$$h(x_1-x_o,y_1-y_o,z_1-z_o) \simeq \frac{e^{jk(z_1-z_o)}\, e^{j\frac{k}{\lambda(z_1-z_o)}\left[(x_1-x_o)^2 + (y_1-y_o)^2\right]}}{j\lambda(z_1-z_o)} \tag{3.10}$$

Fresnel's approximation has the advantage of making the integral in Eq. (3.3) easier to evaluate analytically. When the Fast Fourier Transform algorithm (Section 3.3) is used for the numerical evaluation of Eq. (3.3), Fresnel's approximation makes little difference in the computing time.

3.1.2. The Three-Dimensional Object Model

Figure 3.2 shows the basic arrangement for the evaluation of the diffraction pattern of a three-dimensional object. The diffraction pattern $f_1(x_1,y_1)$ is evaluated as follows; the three dimensional object $f_o(x_o,y_o,z_o)$, located around the coordinate system (x_o,y_o,z_o), is described as a superposition of planar cross sections. The cross sections are taken to be perpendicular to the z axis, at distances $n\Delta z$ from the plane $z = 0$, where $n = 0,1,2,\ldots$ Then the object $f_o(x_o,y_o,z_o)$ can be described by

$$f_o(x_o,y_o,z_o) = \sum_{n=1}^{N} s(z_o-z_{on}) f_{on}(x_{on},y_{on}) \tag{3.11}$$

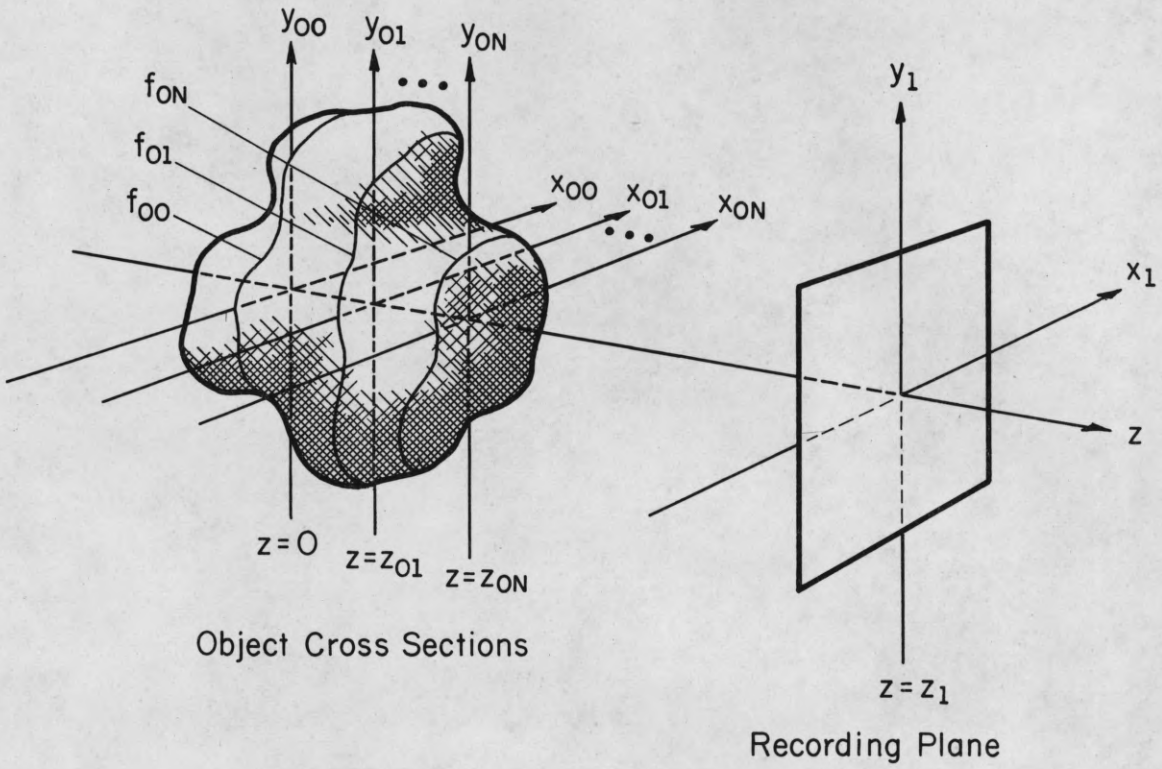

Figure 3.2 Geometrical Arrangement for Recording of Diffraction Pattern

where $f_{on}(x_{on},y_{on})$ is the planar distribution of the object on the nth plane and there is a total of N such planes. The planar distribution functions are space limited, non-negative functions. Each plane consists of a finite number of light transmitting or reflecting points.

Equation (3.11) describes an object whose points radiate all in phase. This is the case of specular reflection or transmission. However, it may not always represent the physical case, where the points may radiate independently from one another. This is the case of diffuse illumination, i.e., the relative phase of the wave scattered by each point is a random variable (Enloe, 1967). In this case the diffusely illuminating object can be represented by the equation

$$f_o(x_o,y_o,z_o) = \sum_{n=1}^{N} \delta(z_o-z_{on}) \sum_{i=1}^{I} \sum_{j=1}^{J} f_{on}(x_o,y_o)\delta(x_o-i\Delta x)\delta(y_o-j\Delta y)d^{j2\pi R_{ij}}$$

$$= \sum_{n=1}^{N} \delta(z_o-z_{on}) \sum_{i=1}^{I} \sum_{j=1}^{J} f_{on}(i\Delta x,j\Delta y)e^{j2\pi R_{ij}} \qquad (3.12)$$

where R_{ij} is a random number such that $0<R_{ij}<1$, and $2\pi R_{ij}$ is the relative phase of the wave scattered from the point scatterer located at $x_o = i\Delta x, y_o = j\Delta y$. The number of scatterers of each planar distribution is I x J. The sampling spatial periods in the x and y directions are $\Delta x,\Delta y$ respectively, i.e., the points are uniformly distributed on each object plane, and for simplicity Δx is taken to equal Δy.

Both cases of diffuse and non-diffuse illumination have been considered. Each case has its own advantages and disadvantages. Diffuse

illumination produces an image covered with a grain-like noise, called "speckle pattern". The speckle pattern or the "Enemy Number One of Holography" as it has been called by the father of holography D. Gabor (1970) degrades the quality of the image and no satisfactory way has been discovered yet for its complete elimination. The same speckle pattern appears when laser light illuminates an object. But diffuse elimination has the advantage of spreading the information about the object upon the hologram plane more evenly than non-diffuse illumination and this increases the dynamic range of the recording medium. Moreover, sections of the hologram can reconstruct the total image although with less resolution. Non-diffuse illumination gives better quality images because of the absence of the speckle pattern.

One of the problems that arises with the description of the object as in Eq. (3.11) is that we can see through the object, i.e., any cross section of the object located behind the Nth plane can be seen from the hologram plane, as if the object was transparent. This is undesirable for opaque objects. Ichioca et al. (1971) have suggested a method of eliminating the "hidden-line" problem for synthesizing a three-dimensional Fourier transform hologram.

In our case the objects were carefully chosen so that subsequent cross sections for $z>0$ would not obstruct the scattered field from the previous cross sections. Work is being carried out at the moment for more complicated objects involving the "hidden line" problem. Points that can not be seen from the hologram are not considered; thus although the "hidden line" problem is eliminated, the parallax is also reduced.

In order to find the diffraction pattern of a three dimensional object we sum up all of the contributions from all the object cross sections on the plane $z = z_1$. For an object described by equation (3.11) by substituting into question (3.3) we obtain the diffraction pattern

$$f_1(x_1,y_1,z_1) \simeq \sum_{n=1}^{N} \iint_{S_{on}} \delta(z-z_{on}) f_{on}(x_{on},y_{on}) \frac{e^{jk|r_1-r_{on}|}}{j\lambda|r_1-r_{on}|} dS_{on} \simeq$$

$$\simeq \sum_{n=1}^{N} \frac{1}{j\lambda(z_1-z_{on})} \iint_{S_{on}} f_{on}(x_{on},y_{on}) e^{jk\sqrt{(x_1-x_{on})^2+(y_1-y_{on})^2+(z_1-z_{on})^2}} dS_{on} \tag{3.13}$$

Again the integration in (3.13) extends over the various cross sections S_{on} from plane $z = z_{oo} = 0$ to $z = z_{on}$. Equation (3.13) holds only for cross sections that are of the type shown in Figure 3.3. That is, every point in these planes can be seen from all points in the diffraction pattern plane.

3.1.3. Numerical Evaluation of the Diffraction Pattern

The complexity of the integral in Eq. (3.13), except in cases where f_{on} represents simple objects (such as points, lines, or simple apertures), rules out any analytic evaluation; thus one has to rely upon numerical techniques for evaluating it. The convolution integral in (3.13) suggests the use of the Fourier Transform (FT). The function f_1 can be written as

$$f_1 = f_o * h \tag{3.14}$$

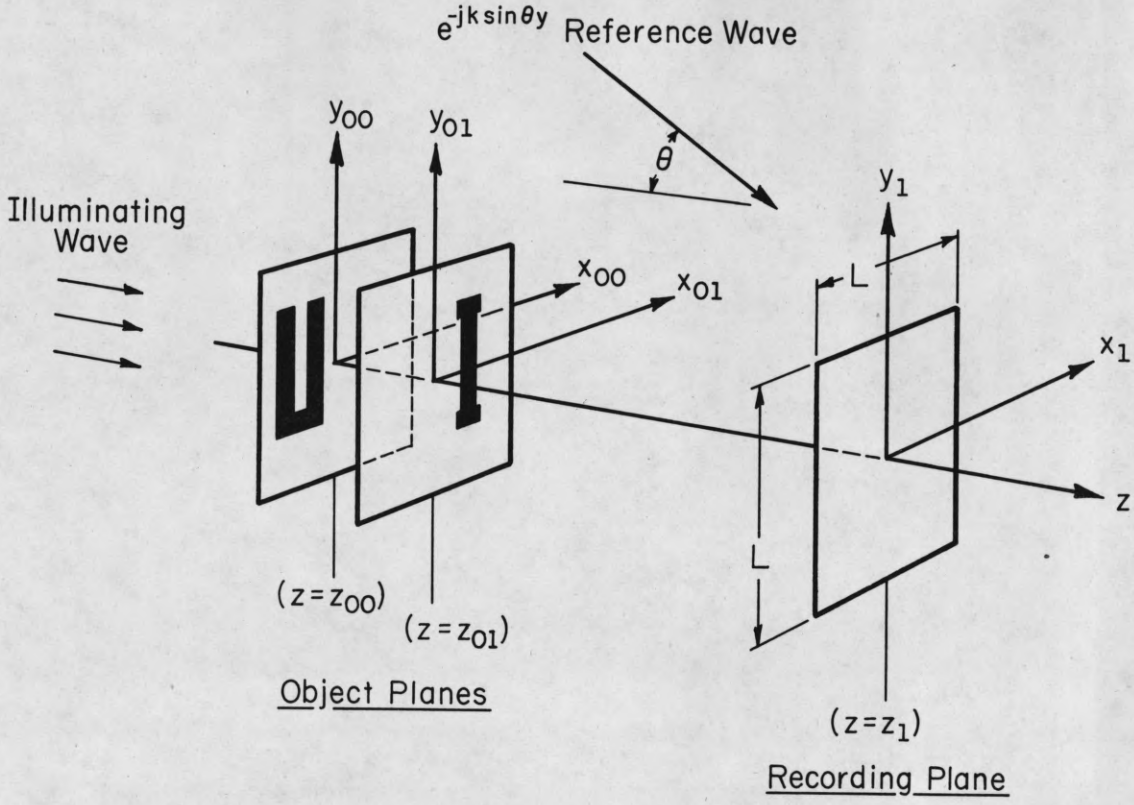

Figure 3.3 Recording of Hologram

where * means convolution. Applying a well known formula (Papoulis, 1962) to (3.14) we have

$$f_1 = F^{-1}(F_1) = F^{-1}(F_o \cdot H) \tag{3.14'}$$

where F_o, H, F_1 are the Fourier transforms of f_o, h, f_1 respectively and F^{-1} designates the inverse FT. For an arbitrary object we have

$$f_1 = \sum_{n=1}^{N} F^{-1}[F_{on} \cdot H_{on}] \tag{3.15}$$

where F_{on}, H_{on} are the FT of f_{on}, h_{on} respectively and N is the number of cross sections. At first glance it would appear that the use of (3.15) instead of (3.13) is not efficient due to the number of operations involved. However the use of the Fast Fourier Transform (FFT) makes the evaluation of Eq. (3.15) more efficient than that of Eq. (3.13).

3.1.4. The Fast Fourier Transform

The introduction of the FFT algorithm discovered by Cooley and Tukey (1965) for the evaluation of the Discrete Fourier Transform (DFT) greatly reduces the computation time required for this calculation. As a consequence, convolution or correlation integrals can be done considerably faster using the FFT than going through the usual integration techniques (Gentleman and Sande, 1966, Stockham, 1966).

Bergland, G. D. (1969) gives a detailed explanation of the use of the FFT in the evaluation of convolution and correlation integrals. The number of operations required to directly evaluate the two-dimensional

Fourier transform represented by an array of N X N samples is N^4. One operation is considered to be an addition and a multiplication. Applying the FFT algorithm to the evaluation of the same N X N matrix a total of $4N^2 \log_2 N$ operations need to be performed. Goodman (1969) gives a tabulation of estimated time required to compute the Fourier transform using both methods; the FFT and direct computation using the IBM 7094 as shown in Table I.

Array Size	Direct Computation	Fast Fourier Transform
N	Time	Time
64 X 64	8 min	3 sec
256 X 256	30 hours	1 min
512 X 512	20 days	5 min
1024 X 1024	1 year	20 min

Comparison of Computation Time : Direct Versus FFT Method.

Table I

The time required by more modern computers is reduced by a factor of more than ~5 of the values indicated on Table I. The time required to evaluate the FT using the FFT of a 128 X 256 array in the IBM 360/75 is approximately 13 sec. The time reduction advantages of the use of FFT over the direct evaluation of DFT can be seen on Table I. It must be kept in mind, however, that the "blind" use of FFT in the evaluation of any type of function can lead to serious errors.

Bergland, G. D. (1969), Ransom, P. L. (1969) have described some of the pitfalls of the use of FFT. Since the FFT is a fast way of evaluating

the DFT, before the FFT is applied caution must be exercised to make sure that the DFT can approximate the continuous FT. One of the unavoidable errors that is introduced is that a space limited function is assumed to be bandlimited. However, it turns out that such an error is small due to the fact that $x_{max} f_{x_{max}}$ is assumed much larger than one (Cochran, Cooley, et.al., 1967).

3.2. Simulation

3.2.1. Background

The geometrical configuration for the digital simulation is shown in Figure 3.3. It consists of a three dimensional object illuminated by a coherent wavefront. The diffracted waves together with a reference wave impinge upon the hologram plane. The procedure for evaluating and recording the diffraction pattern is similar to the one described by Lesem, et al. (1967), except that we consider a three dimensional object which is contracted in the recording process to avoid the longitudinal distortion inherent in the process, as explained in Chapter 2.

The digital evaluation of the intensity $I(x_1,y_1)$ is performed according to the flow diagram shown in Figure 3.4. The original object is shown in Figure 3.5. It consists of the two letters, U and I; they are located at different planes as shown in Figure 3.3 but were plotted coplanar on the CRT for illustrative purposes. The object is such that all points of it are visible from every point in the hologram plane. The points that are not visible present a problem because although they are obscurred in the recording process, if we follow the above approach they will be visible in the reconstruction image. Other objects have been examined where there are non-visible points.

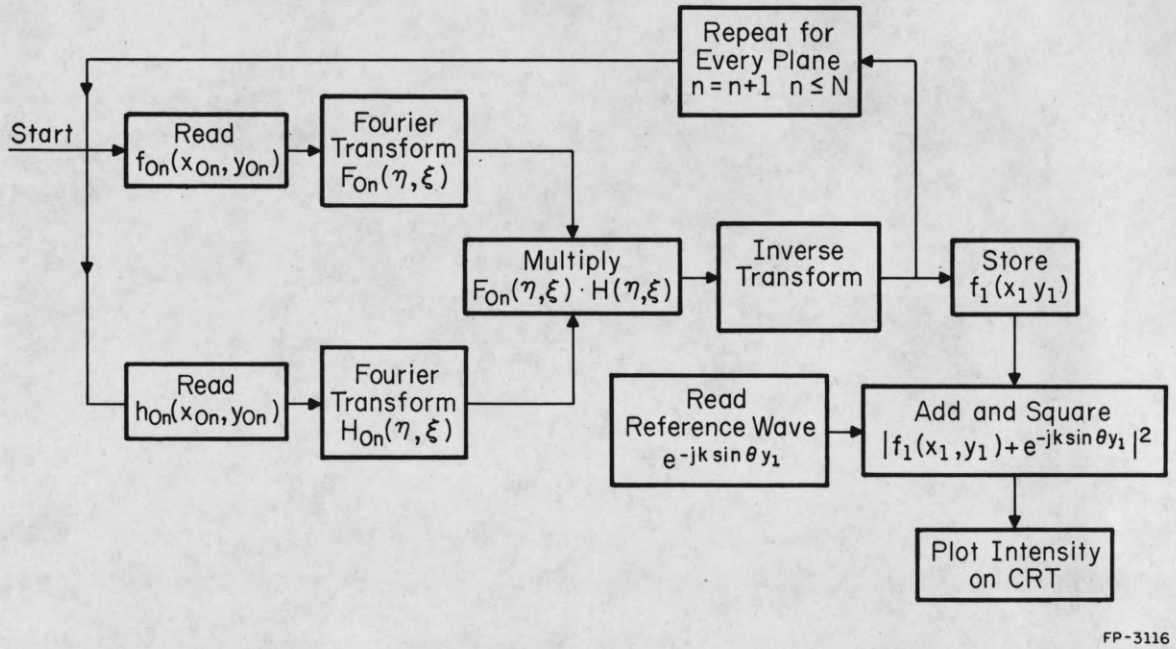

Figure 3.4 Flow Diagram for the Recording Process

Figure 3.5 Original Object. (The two letters U and I are located at different planes as shown in Figure 3.3)

Similar work has been reported by Ichioka et.al., (1971) forming three-dimensional Fourier-transform holograms.

Every cross section at the object has 128 X 128 resolution elements. The area of planes over which the sampling is done is 8 X 8 cm^2. The wavelength is .04 cm. The sampling of the propagator function (h), was also performed in the same manner as for the object at 128 X 128 points. It must be pointed out that the object function f_{on} and propagation function h are complex, thus the arrays for the 128 X 128 sampling points are of size 256 X 128. The function f_{on} representing the transmission distribution of the nth plane, and the propagator h are Fourier transformed and then multiplied. The inverse Fourier transform of the product is taken and the result represents the function $f_1(x_1,y_1,z_1)$. The reference wave is sampled and added to $f_1(x_1, y_1,z_1)$. Then the intensity is plotted on the CRT.

3.2.2. Sampling of the Diffraction Pattern

The diffraction pattern $f_1(x_1,y_1,z_1)$ is evaluated according to the flow diagram shown in Figure 3.4. The reference wave is given by

$$U_r = Se^{-jk \sin\theta y_1} \tag{3.16}$$

where S is a constant and θ is the angle that the propagation vector k makes with the normal to the hologram. Since the object wave at $z = z_1$ is given by $f_1(x_1,y_1,z_1)$ the intensity is

$$I(x_1,y_1,z_1) = \left| f_1(x_1,y_1,z_1) + Se^{-jk \sin\theta y_1} \right|^2 . \tag{3.17}$$

In synthetic holography the recording of the intensity is carried out by digital sampling of the intensity $I(x_1,y_1,z_1)$. In order for the discrete sampling array to represent the intensity I, the spatial rate of sampling must be such that it satisfies the sampling theorem (O'Neill, 1962). That is: at least two samples per cycle of the highest spatial frequency component in the intensity $I(x_1,y_1,z_1)$ must be taken. Thus we first have to find the highest spatial frequency of the interference pattern. The object wave can be considered to be made up of many elementary point sources. For simplicity we will find the spatial frequency for one such point source located at (x_o,y_o,z_o), and a plane wave reference source as shown in Figure 3.6. At the recording plane the spherical wave originating from the point (x_o,y_o,z_o) is

$$U_o(x_1,y_1,z_1) = Ae^{jk[(x_1-x_o)^2 + (y_1-y_o)^2 + (z_1-z_o)^2]^{\frac{1}{2}}} . \qquad (3.18)$$

Using the Fresnel's approximation (Eq. 3.9) in (3.18) and setting $z_o = 0$ as our reference zero point we have

$$U_o(x_1,y_1,z_1) \approx Ae^{jkz_1} e^{j\frac{\pi}{\lambda z_1}[x_1-x_o)^2 + (y_1-y_o)^2]} \qquad (3.19)$$

Superimposing on $U_o(x_1,y_1,z_1)$ the reference wave $U_r(x_1) = Se^{-jk \sin\theta x1}$ we have the intensity

$$I = \left| Ae^{jkz_1} e^{j\frac{\pi}{\lambda z_1}[(x_1-x_o)^2 + (y_1-y_o)^2]} + Se^{-jk \sin\theta x_1} \right|^2$$

$$= A^2 + S^2 + 2AS \cos[\varphi(x_1,y_1)] \qquad (3.20)$$

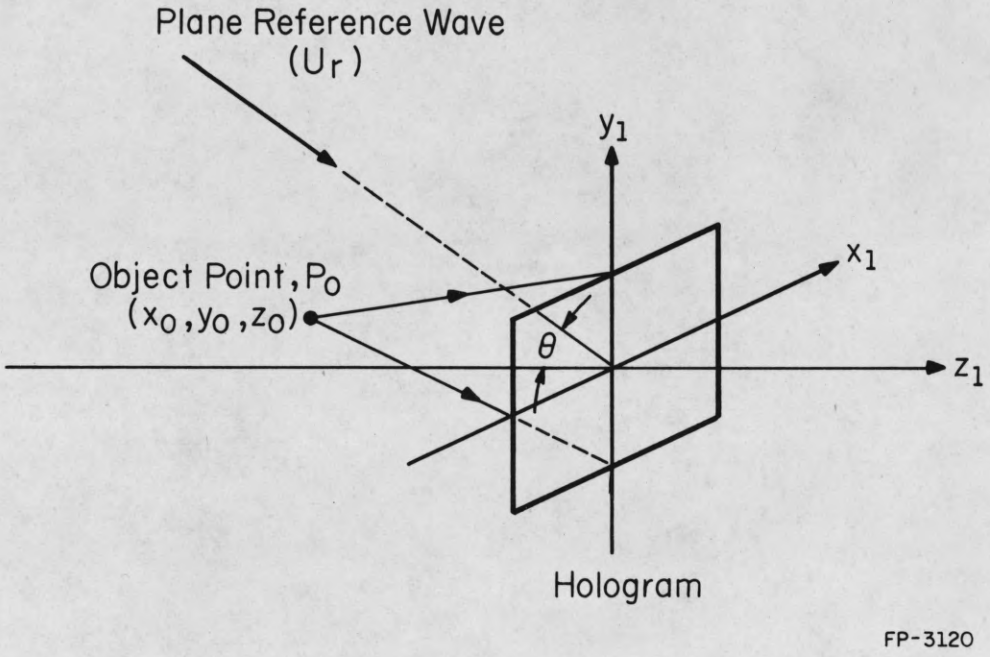

Figure 3.6 Diagram for Construction of a Hologram of a Point Object

where

$$\varphi(x_1,y_1) = kz_1 + \frac{\pi}{\lambda z_1}\left[(x_1-x_o)^2 + (y_1-y_o)^2\right] - k\sin\theta y_1 \qquad (3.21)$$

The spatial frequencies f_{x_1}, f_{y_1} are

$$f_{x_1} = \frac{1}{2\pi}\frac{\partial\varphi}{\partial x_1} = -\frac{x_o-x_1}{\lambda z_1} \qquad (3.22)$$

$$f_{y_1} = \frac{1}{2\pi}\frac{\partial\varphi}{\partial y_1} = -\frac{y_1-y_o}{\lambda z_1} - \frac{\sin\theta}{\lambda z_1} \quad . \qquad (3.23)$$

Equations (3.22) and (3.23) show that different spatial frequencies occur in the x,y directions. In order for the sampling theorem to be satisfied the sampling periods $\Delta x, \Delta y$ must satisfy the following

$$\Delta x \leq \frac{1}{2f_{x_{1max}}} \qquad (3.24)$$

$$\Delta y \leq \frac{1}{2f_{y_{1max}}} \qquad (3.25)$$

In our case L = 8 cm, where L is the overall dimension of the square size hologram, x_{1max} = 4 cm, x_o = -1.3 cm, $\theta = 10^o$, λ = .04 cm, z_1 = 2 cm, we find $f_{x_{1max}}$ = 14.25. The sampling period $\Delta x = \Delta y = \frac{L}{128} = \frac{8\text{ cm}}{128} = .0625$ cm. Thus we can see from (3.24), (3.25) that $I(x_1,y_1)$ is undersampled only at the edges of the hologram. In order to avoid the undersampling problem the

sampling interval must decrease and therefore the number of sampling points will have to increase. But computer storage capacity sets a limit as to the number of points that can be used. Equation (3.23) shows that the angle θ that the incident reference wave makes with the normal to the hologram plane is also limited because f_{y_1} is limited. By limiting the angle θ to a small value the final image wave may not be separated from the "on-axis" wave (first two terms in equation 2.6). An optical system described in Chapter 4 is used to separate the two waves, the image wave from the "on-axis" wave. Also, by limiting the spatial frequencies for reasons discussed above, the angular field of view, and the size of the object and image are also limited.

The numerical evaluation of the diffraction pattern was performed in an IBM model 360/75 computer and the time required for the computation of the object shown in Figure 3.3 is ~90 seconds. The data of the sampled intensity were recorded on a magnetic tape and transferred to a Control Data Corporation model 1604 computer. This computer was used to drive a high resolution, high contrast cathode ray tube capable of displaying 4096 X 4096 points on a 2 X 2 in^2 area. The level of intensity of the points can be any integer value from zero to 255. Because we were limited by the computer memory, we evaluated only 128 X 128 points and plotted them on the CRT in a one square inch with plotting time of approximately 40 seconds. The CRT display is shown in Figure 3.7. The hologram was reduced optically to a quarter of its initial size and recorded on film. The final hologram transparency is of size .635 X .635 mm^2. This transparency is used for the optical reconstruction of the image.

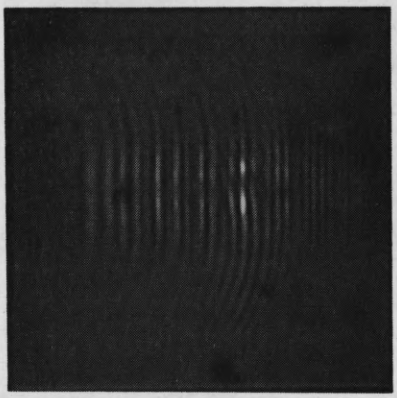

Figure 3.7 Hologram of Object Shown in Figure 3.3

4. OPTICAL RECONSTRUCTION

4.1. Optical Setup

Figure 4.1 shows a diagram of the experimental setup used for the optical reconstruction. The holographic transparency is illuminated by a collimated beam originating from a He-Ne laser. As pointed out in Chapter 3, the angle θ may not exceed a certain value because of the limit imposed upon by the sampling period. Since the angle θ cannot be made very large in the recording process, the angle between the first terms ("on axis waves") in Eq. (2.4) and the fourth term (real image wave) in (2.4) is very small and the image wave overlaps with the "on-axis" waves. The system of the two lenses and the filter as shown in Figure 4.1 is used for filtering out the "on-axis" wave.

4.2. Filtering

The hologram is a mesh of 128 X 128 variable intensity points. It can be represented as a two-dimensional grating by

$$h_s(x,y) = h(x,y) \sum_{n=-\frac{N}{2}}^{\frac{N}{2}-1} \sum_{m=-\frac{M}{2}}^{\frac{M}{2}-1} \delta(x-nd)\delta(y-nd) =$$

$$= \sum_{n=-\frac{N}{2}}^{\frac{N}{2}-1} \sum_{m=-\frac{M}{2}}^{\frac{M}{2}-1} h(nd,md)\delta(x-nd)\delta(y-nd) \qquad (4.1)$$

where $d = \Delta x = \Delta y$ is the sampling period. The hologram is placed in the front focal plane of the lens L_1. The plane wave impinging upon the hologram

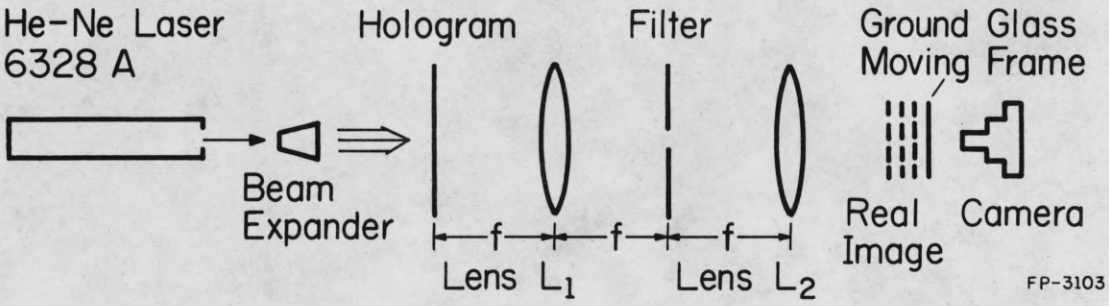

Figure 4.1 Arrangement for Optical Reconstruction

is diffracted not only bythe hologram but also by the grating satisfying the grating equation (we consider only one dimension for simplicity)

$$d \sin \varphi = n\lambda \tag{4.2}$$

where $d = \frac{L}{N}$, L being the overall length of the grating (hologram), N being the number of the lines and n is an integer, $n = 0, \pm 1, \pm 2, \ldots$ For L = .635 cm, N = 128, $\lambda = 6328\text{Å}$ we find

$$\varphi = \sin^{-1}\left(\frac{n\lambda N}{L}\right) = \sin^{-1}\{n(.128)\} \tag{4.3}$$

Figure 4.2 shows the distribution of the various diffraction orders. If the hologram was not sampled, only the zero order "on-axis" and "off-axis" distributions would be present (Cathey, 1968).

A thin lens has the property that a transparency located on its front focal plane and illuminated by a plane wave produces in its back focal plane a complex amplitude distribution which is the Fourier transform of the transparency transmittance (Collier et al., 1971). Thus we apply the Fourier transform to $h_s(x,y)$ Eq. (4.1) to find the field amplitude distribution on the back focal plane of L_1. Let $H_s(f_x,f_y)$, $H(f_x,f_y)$ be the Fourier transorms of $h_s(x,y)$, $h(x,y)$ respectively. Then applying the convolution theorem to (4.1) we obtain

$$H_s(f_x,f_y) = H(f_x,f_y) * F\left[\sum_{n=-\frac{N}{2}}^{\frac{N}{2}-1}\sum_{m=-\frac{M}{2}}^{\frac{M}{2}-1} \delta(x-nd)\delta(y-nd)\right] \tag{4.4}$$

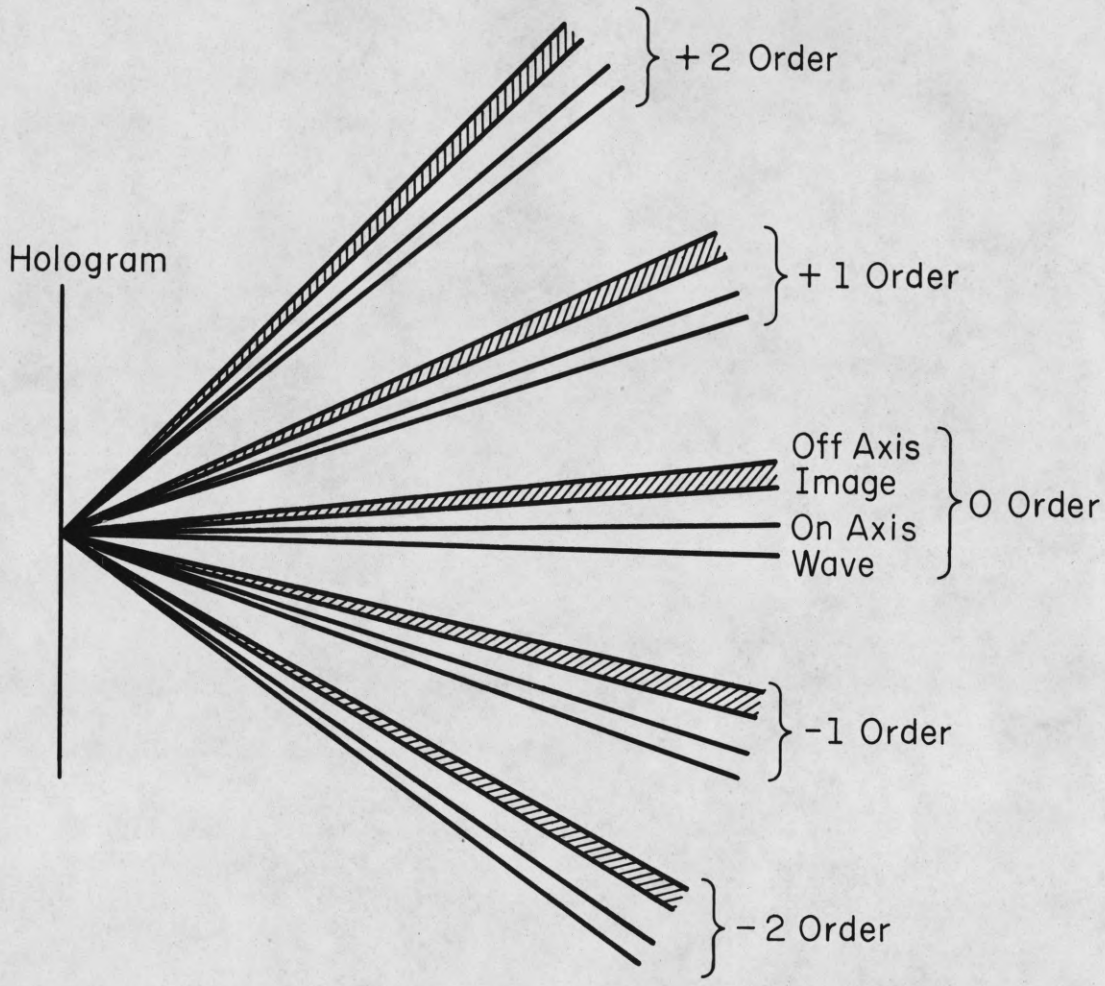

Figure 4.2 Distribution of Various Orders of Diffraction of a Sampled Hologram

Since

$$F\Big[\sum_{n=-\frac{N}{2}}^{\frac{N}{2}-1}\sum_{m=-\frac{M}{2}}^{\frac{M}{2}-1}\delta(x-nd)\delta(y-nd)\Big] = \frac{1}{d^2}\sum_{n=-\frac{N}{2}}^{\frac{N}{2}-1}\sum_{m=-\frac{N}{2}}^{\frac{M}{2}-1}\delta(f_x-\tfrac{n}{d})\delta(f_y-\tfrac{m}{d}) \qquad (4.5)$$

by substituting in (4.4) we find

$$H_s(f_x,f_y) = H(f_x,f_y) * \frac{1}{d^2}\sum_{n=-\frac{N}{2}}^{\frac{N}{2}-1}\sum_{m=-\frac{N}{2}}^{\frac{M}{2}-1}\delta(f_x-\tfrac{n}{d})\delta(f_y-\tfrac{m}{d}) =$$

$$= \sum_{n=-\frac{N}{2}}^{\frac{N}{2}-1}\sum_{m=-\frac{M}{2}}^{\frac{M}{2}-1} H(f_x-\tfrac{n}{d}\ ,\ f_y-\tfrac{m}{d}) \qquad (4.6)$$

Equation (4.6) indicates that the various diffraction orders are spatially separated if the following inequalities hold

$$d \le \frac{1}{B_x} \qquad (4.7a)$$

$$d \le \frac{1}{B_y} \qquad (4.7b)$$

where $2B_x$, $2B_y$ are the widths in the f_x, f_y directions (Goodman, 1968). The function $H_s(f_x,f_y)$ is assumed to be bandlimited. By using a spatial filter as shown in Figure (4.1) the higher diffraction orders are removed. We prefer to extract the image wave from the zero diffraction order because it is the term of the highest intensity. Due to the fact that the image wave makes a small angle with the "on-axis" wave as shown in Figure 4.2, the image wave is slightly displaced from the optical axis in the Fourier transform

plane. This enables us to remove all of the unwanted spectral components by filtering and be left with the image wave only. The second lens L_2 performs the Fourier transform of the distribution of its front focal plane which in this case after the filtering it is only the spectral distribution of the image wave. The image is formed further back from the back focal plane of lens L_2.

The set up shown in Figure 4.1 enables one to photograph any cross section of the real image by projecting it on a screen and focusing the camera appropriately. Figures 4.3 (a), (b) show such cross sections. It can be seen that in Figure 4.3(a) part of the object (the letter U) is out of focus, while in Figure 4.3(b) the letter I is out of focus. The object consists of two letters U and I located on two different planes. The wavelength ratio $\mu = \frac{\lambda_1}{\lambda_2}$ is 1/635 for laser light of wavelength $\lambda_1 = 6328\text{Å}$ and sub-optical wave of wavelength $\lambda_2 = .04$ cm. The hologram has an area of 8×8 cm^2 and after reduction its area becomes $.635 \times .635$ cm^2. Therefore the reduction ratio m is $\frac{1}{12.6}$. The distance from the letters U, I to the hologram in the recording process is 20 cm and 16 cm respectively. The distances of the images of the letters U, I from the hologram are 80 cm and 64 cm respectively. Thus the longitudinal dimension is 16 cm. If there was no longitudinal distortion the longitudinal dimension would be $\frac{4}{12.6} = 3.17$ mm. In another case we applied a longitudinal distortion of the object in the recording process, i.e., we contracted the object by a factor of 50. In this case there was not any longitudinal distortion but due to the large depth of focus (described in the next section) the object appeared as a two dimensional one. More experiments are under way to reduce the longitudinal magnification without having

(a) (b)

Figure 4.3 (a) (b). Optically Reconstructed Images.
In (a) the Letter U is Out of Focus
In (b) the Letter I is Out of Focus

a large depth of focus.

The virtual image also displays its three dimensional characteristics. As is the case with the real image, the virtual image is also located close to the "on-axis" term leading to difficulty in observing the image. Moreover, higher order virtual images are present for the same reasons as described in the case of real images.

4.3. Depth of Focus

One of the disadvantages in three-dimensional image displaying using synthetic holograms is that the depth of focus of the image is large compared to the depth (longitudinal dimension) of the object. This occurs when the scaling factor m is not equal to wavelength ratio μ. The depth of focus in conventional imaging is defined as being the maximum permissible movement away from the ideal image plane (object plane remains stationary) which may be made without causing a serious deterioration of the image (Longhurst, 1967). It is given by (Born and Wolf, 1970)

$$\Delta Z' = \pm 2\left(\frac{f}{D}\right)^2 \lambda \tag{4.8}$$

where λ is the wavelength and f,D are the lens focal length and aperture respectively. The same formula can be applied to holography and (4.8) can be written as

$$\Delta Z' = \pm 2\left(\frac{z_i}{D}\right)^2 \lambda_2 \tag{4.9}$$

where D is the aperture of the hologram, z_i is the image to hologram distance and λ_2 is the viewing wavelength. It can be seen from (4.9) that the high

$\frac{z_i}{D}$ ratio of synthetic holograms as compared to low $\frac{f}{D}$ ratio in conventional imaging is responsible for the large depth of focus. Since $z_i = \frac{m^2}{\mu} z_o$ (Eq. 2.15), $\lambda_2 = \mu\lambda_1$, $D_2 = mD_1$, by substituting in Equation (4.9) we have

$$\Delta Z' = \pm 2\left(\frac{z_o}{D_i}\right)^2 \lambda_1 \frac{m^2}{\mu} . \qquad (4.10)$$

It can be seen in (4.10) that for a smaller object to hologram distance a smaller depth of focus is obtained. Typically for z_o = 16 cm, D_1 = 8 cm, λ_1 = .04 cm, m = $\frac{1}{12.6}$, $\mu = \frac{1}{635}$ we obtain $\Delta z' = \pm 1.28$ cm. This depth is field is large compared to the depth of an object that might be of the order of a few centimeters. The object will appear two dimensional due to a large depth of focus. Figure 4.4 shows the two letters as being on the same plane.

The depth of focus limits our capability of making a true three-dimensional image by contracting the object in the recording process by a large factor. But we are still able to reduce the longitudinal magnification by an amount that the depth of focus permits. This in turn can be very useful in cases where the scaling factor m is close to μ.

The cause of the large depth of focus (and consequently the large depth of field) can be traced back to the recording process where the aperture of the hologram is small compared to the recording wavelength (Mueller et.al., 1969). Larger hologram aperture and smaller wavelength will reduce the depth of focus but it will require an increase in computation time and memory capacity of the computer. Moreover, the increase of aperture will increase the angular field of view of the image.

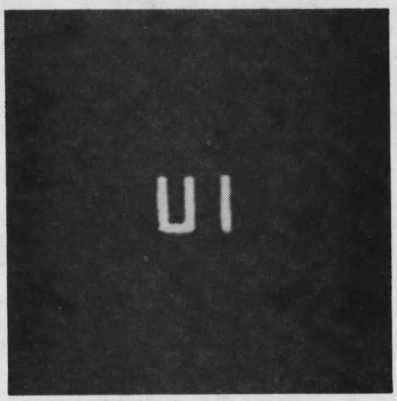

Figure 4.4 Optically Reconstructed Image.
Both Letters are in Focus

5. DIGITAL RECONSTRUCTION

5.1. Recording of Diffraction Pattern

When optical reconstruction is applied to acoustic or microwave diffraction patterns, a reference wave is superimposed upon the object diffraction pattern to form an interference pattern. The intensity of the interference pattern is sampled and displayed on a CRT. An optical transparency of the displayed hologram is made and scaled down. The transparency is illuminated by a coherent light source and an optical image of the initial object is obtained. As it was pointed out in Chapter 2, the optical image is extremely small and longitudinally distorted. This prompted the development of methods for digital reconstruction. The literature on the various recording and reconstruction techniques is very extensive (Metherell et al., 1969, Preston and Kreuzer, 1967, Aoki, 1967, Mueller, 1971).

When digital reconstruction is applied no reference wave is required in the recording process. This of course is the case where the linear detectors used to sample the diffraction pattern can detect not only its magnitude but also its phase. At microwave and acoustic frequencies this is indeed possible. Thus the recorded diffraction is called a "hologram" because total recording occurs although no reference wave is used as is the case of ordinary optical holograms.

The complex wavefront $f_1(x_1,y_1,z_1)$ (Chapter 3) can be directly recorded using acoustic or microwave probes, depending upon the type of wave used, or two dimensional array detectors. The complex array representing the amplitude and phase of $f_1(x_1,y_1,z_1)$ is stored in the computer for further

processing and digital reconstruction.

For our computer simulation the forward diffraction pattern is evaluated using the same method that was applied to synthetic holograms as described in Chapter 3 (Figure 3.4), except the reference wave is omitted. The function $f_1(x_1,y_1,z_1)$ is given by

$$f_1(x_1,y_1,z_1) = f_o(x_o,y_o,z_o)*h(x_o,y_o,z_o) \tag{5.1}$$

where * denotes convolution, and $f_o(x_o,y_o,z_o)$ represents the object, $h(x_o,y_o,z_o)$ is the forward propagator and $f_1(x_1,y_1,z_1)$ is the scattered field of the object $f_o(x_o,y_o,z_o)$ at $z = z_1$ plane (Chapter 3). The function $f_1(x_1,y_1,z_1)$ is sampled at 128 X 128 points and the 128 X 256 array is stored in the computer.

5.2. Theoretical Reconstruction

Figure 5.1 shows the geometry for the reconstruction process. Our aim is to reconstruct the object $f_o(r_o)$ from its diffraction pattern $f_1(r_1)$. Rayleigh's diffraction theory for inverse propagation is applied as described by Lalor (1968). Similar techniques have been reported by Shewell and Wolf (1968), Mittra and Ransom (1967). The given field distribution at $z = z_1$ is $f_1(r_1)$, and from $f_1(r_1)$ we want to determine the field distribution $f_o(r_o)$ at the various planes $z_o = z_{o1},z_{o2},\ldots,z_{on}$, where $z_o \geq 0$. The function $f_o(r_o)$ is given by

$$f_o(r_o) = \iint_{S_1} f_1(r_1)g(r_o,r_1)dS_1 \ . \tag{5.2}$$

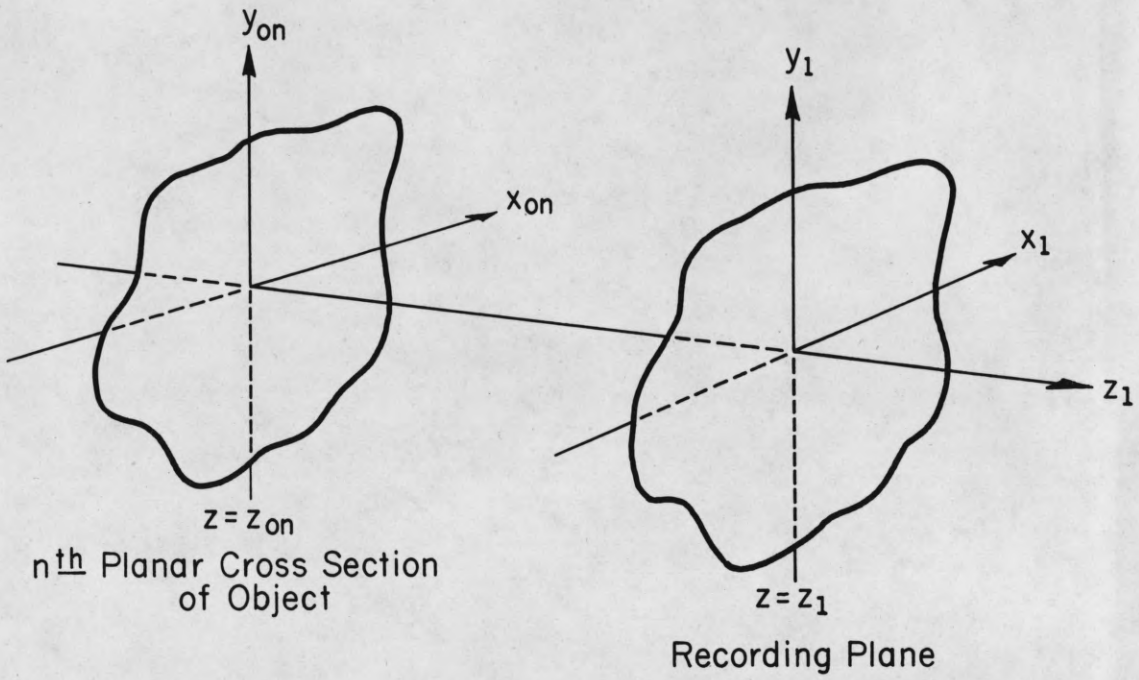

Figure 5.1 Reconstruction Geometry

The Kernel $g(r_o,r_1)$ is

$$g(r_o,r_1) \simeq -\frac{1}{2\pi}\frac{\partial}{\partial z_1}\left[\frac{e^{-jk|r_1-r_o|}}{|r_1-r_o|}\right] = -\frac{1}{2\pi}\frac{\partial}{\partial z_1}\frac{e^{-jk[(x_1-x_o)^2+(y_1-y_o)^2+(z_1-z_o)^2]^{\frac{1}{2}}}}{[(x_1-x_o)^2+(y_1-y_o)^2+(z_1-z_o)^2]^{\frac{1}{2}}}$$

$$= -\frac{1}{2\pi}\left[\frac{ik(z_1-z_o)(-2)}{2|r_1-r_o|} - \frac{(z_1-z_o)}{|r_1-r_o|^2}\right]\frac{e^{-jk|r_1-r_o|}}{|r_1-r_o|}$$

$$= \frac{1}{2\pi}\frac{(z_1-z_o)}{|r_1-r_o|^2}e^{-jk|r_1-r_o|}\left[jk + \frac{1}{r_1-r_o}\right] . \qquad (5.3)$$

For large $|r_1-r_o|$ the second term in (5.3) can be ignored. Thus we have

$$g(r_o,r_1) \simeq \frac{e^{-jk|r_1-r_o|}}{-j\lambda(z_1-z_o)} . \qquad (5.4)$$

Finally, after all of the approximations shown above are made by substituting (5.4) into (5.2) we have

$$f_o(r_o) \simeq \frac{1}{-j\lambda(z_1-z_o)}\iint f_1(r_1)\, e^{-jk|r_1-r_o|}\, dS_1 . \qquad (5.5)$$

Equation (5.5) is applied to the reconstruction of the three dimensional object. In such a case (5.5) becomes

$$f_{on}(x_{on},y_{on},z_{on}) \simeq \frac{1}{-j\lambda(z_1-z_{on})}\iint f_1(r_1)\, e^{-jk|r_1-r_{on}|}\, dS_1 \qquad (5.6)$$

The subscript n refers to the nth planar distribution of the object.

Again we evaluate the integral equation (5.6) using the FFT. For the nth cross section of $f_o(r_o)$ we have

$$f_{on}(x_{on},y_{on},z_{on}) \simeq F^{-1}\{F[f_1(r_1)]\ F[\frac{e^{-jk|r_1-r_{on}|}}{j\lambda(z_1-z_{on})}]\} \ . \qquad (5.7)$$

It can be seen from (5.6) that for any value of z_1-z_{on} we can propagate backward to any desired distance from the diffraction pattern. If z_1-z_{on} is not known a trial and error type approach can be applied. Such would be the case in physically recording the diffraction pattern of an object that is inside an opaque medium, such as the human body, opaque liquid, etc. This problem can be approached as follows: we propagate backward using several different distances until we have some indication of the location of the object. Then we evaluate many cross sections at such distances and display them on a CRT.

5.3 Experimental Results

Figure 5.2 shows the diffraction pattern for the object shown in Figure 3.3. The evaluation of $f_{on}(r_{on})$ is performed according to the flow diagram shown in Figure 5.3. The complex valued function $f_{on}(r_{on})$ evaluated at a particular plane and plotted on a CRT represents a cross section of the original object. Some noise from other cross sections that are "out of focus" is also presented. It must be pointed out that for the reconstruction of plane distribution of the image the FFT is applied twice, as can be seen from the flow diagram, since $F[f_1(r_1)]$ is stored. Figures 5.4 (a), (b) show cross sections of the reconstructed image. It can be seen in 5.4 (a) that the letter U is out of focus and in 5.4 (b) the letter I is out of focus. If we propagate backward to planes of z that do not contain the image we observe the object of parts of it being out of focus. Figures 5.5 (a), (b) show such cross sections for z = -12 cm and z = -24 cm. The true positions of the two letters I, where U-16 cm, -20 cm respectively.

If the object was considered to be diffusely illuminated as a represented by Eq. (3.12) then the speckle pattern appears in the reconstructed images. Figure 5.6 shows the diffraction pattern for the diffusely illuminated object of Figure 3.3. The reconstructed cross sections for a diffusely illuminated object are shown in Figures 5.7 (a),(b). Figures 5.8 (a),(b) show cross sections for a diffusely illuminated object. Figures 5.8 (a), (b) show cross sections of object a z=-12cm, -24 cm. Comparing the two cases of diffusely and non-diffusely illuminated objects (Figures 5.4, 5.7) we see that the non-diffuse illumination case gives better images with more clarity than the diffuse illumination case. However, the diffusely illuminated planes that are out of focus do not show up distinctly. In practice when real objects are used with a few exceptions diffuse illumination is unavoidable.

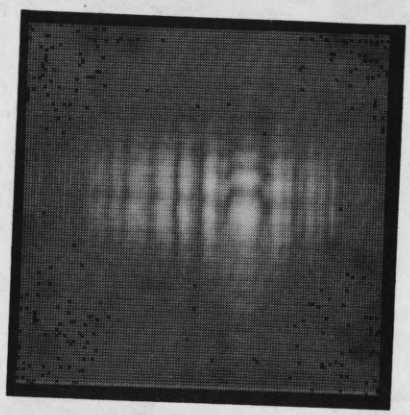

Figure 5.2 Diffraction Pattern of Object
Shown in Figure 3.3. Non-Diffuse Illumination Was Used

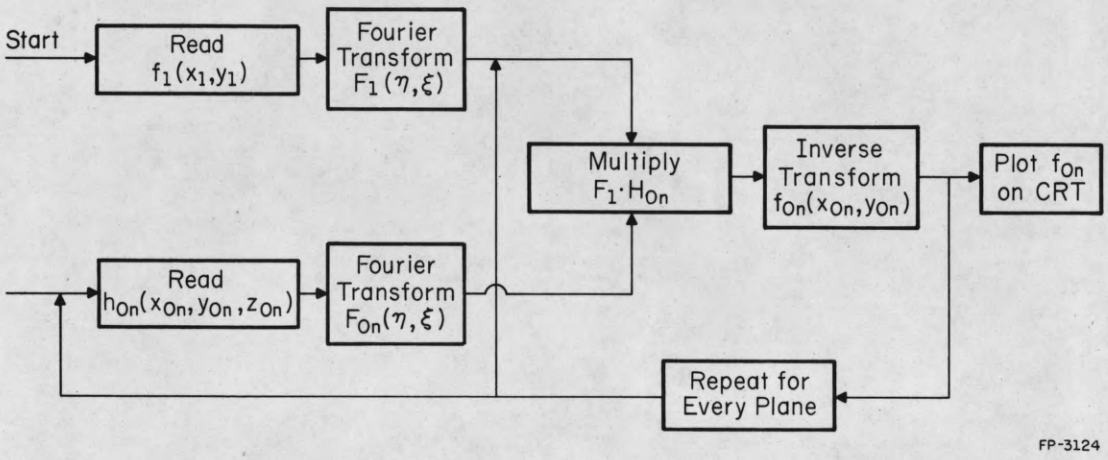

Figure 5.3 Flow Diagram for Digital Reconstruction

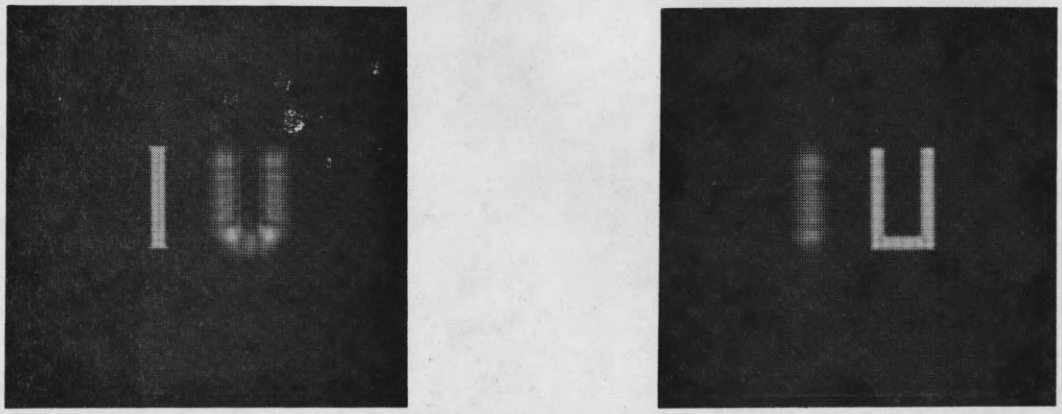

(a)

Letter U Out of Focus

(b)

Letter I Out of Focus

Figure 5.4 (a) (b). Digitally Reconstructed Cross Sections of Object from Diffraction Pattern Shown in Figure 5.2. Non-Diffuse Illumination Was Used.

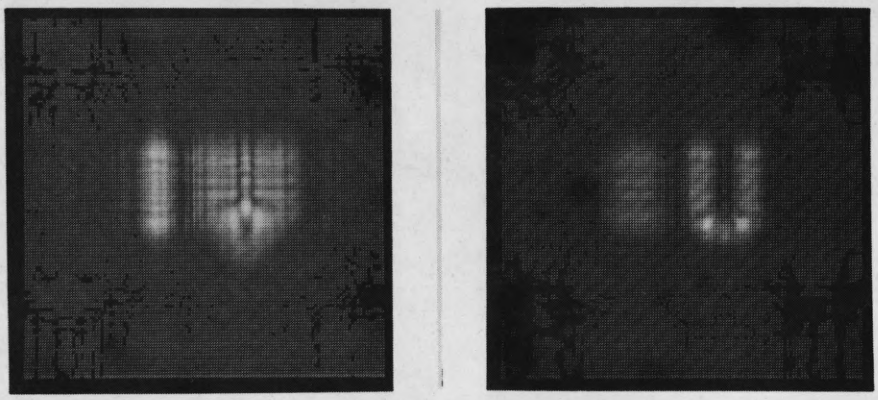

(a) (b)

Figure 5.5 (a) (b). Digitally Reconstructed Cross Sections at z = -12 cm and z = -24 cm for Figures (a), (b) Respectively. Both Planes are Out of Focus. The True Positions of the Letters U and I were -20 cm, -16 cm Respectively. Non-diffuse Illumination Was Used.

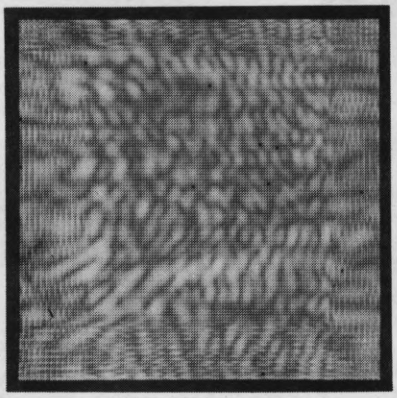

Figure 5.6 Diffraction Pattern of Object
Shown in Figure 3.3. Diffuse Illumination Was Used.

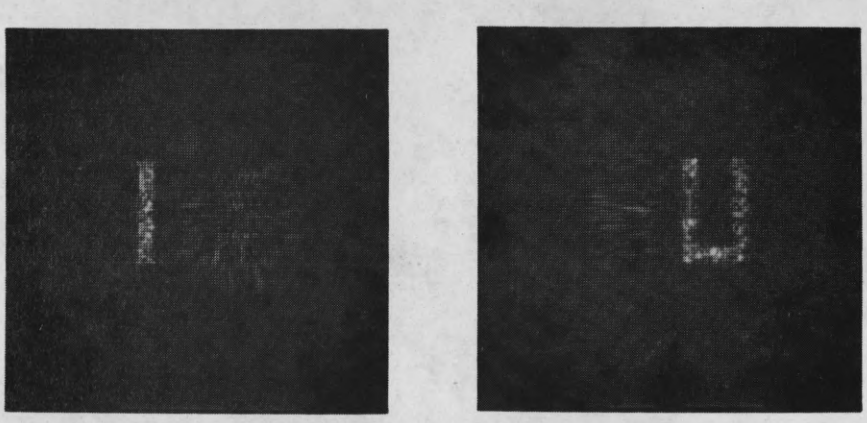

(a)

Letter U Out of Focus

(b)

Letter I Out of Focus

Figure 5.7 (a) (b). Digitally Reconstructed Cross Sections of Object from Diffraction Pattern Shown in Figure 5.6. Diffuse Illumination Was Used.

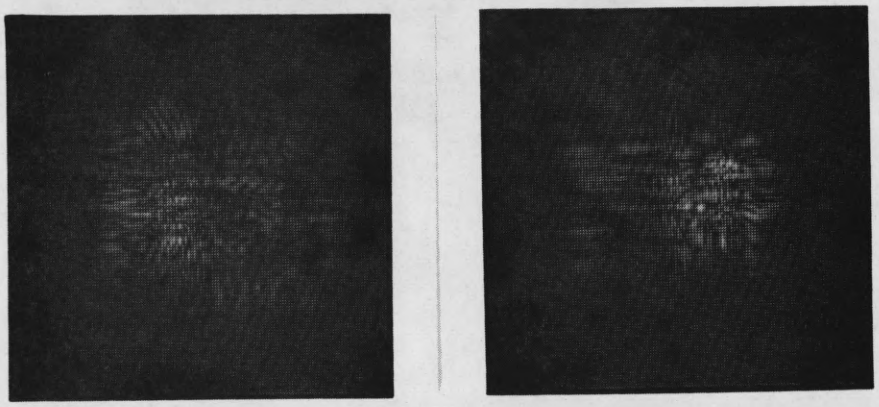

(a) (b)

Figure 5.8 (a) (b). Digitally Reconstructed Cross Sections at z = -12 cm and z = -2u cm for Figures (a), (b) Respectively. Both Planes are Out of Focus. The True Positions of the Letters U and I were at - 20 cm, -16 cm, Respectively. Diffuse Illumination Was Used.

Since the final form of the image that we obtain by using digital reconstruction is in digital form, the data can be further operated upon before displaying. The contrast of the image can be improved by quantizing the intensity to two or more levels. Figures 5.9, 5.10, 5.11, 5.12 show various such quantizations of the images of the Figures 5.4 (a), (b), 5.7 (a), (b). Moreover image enhancement can be applied before the final displaying on the CRT. Thus more information can be extracted about the object (Andrews 1970, Huang et al., 1971).

By using digital reconstruction, the photographic processing and reduction of the hologram required for optical reconstruction is eliminated. Moreover almost instant display of the reconstructed image is possible. A fast acoustic or microwave scanner, or a two dimensional acoustic detector connected to a fast large capacity computer can obtain the sampled data of the diffraction pattern. Then the various cross sections can be evaluated and displayed on a computer driven CRT. The delay time will be the time required by the scanner plus the computation time of the computer plus the display time of the CRT. The delay time will be the time required by the scanner plus the computation time of the computer plus the display time of the CRT. Figure 5.13 shows such a proposed set up. Using digital reconstruction we do not display the three dimensional object, rather different cross sections of it. The three dimensional optical reconstruction from non-optical holograms has the disadvantages (pointed out in Chapter 3) such as giving small image and longitudinal distortion. The corresponding disadvantage of digital reconstruction is that the number of data points that can be handled is limited. However, future fast and high capacity computers should alleviate this problem.

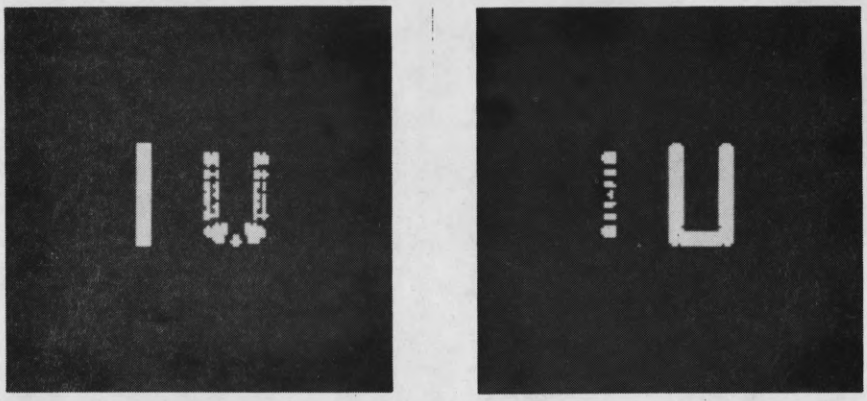

(a) (b)

Figure 5.9 (a) (b). Two Level Quantization in the Intensity of Figures 5.4 (a) (b). Intensity of Points I = 250 if $I \geq 200$. (Scale 0 → 255).

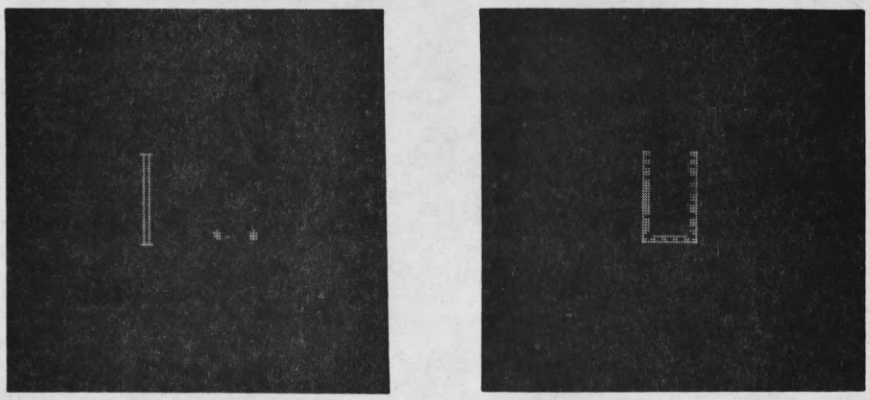

(a) (b)

Figure 5.10 (a) (b). Two Level Quantization in the Intensity of Figures 5.4 (a) (b). Intensity of Points I = 250 if $I \geq 150$. (Scale 0 → 255).

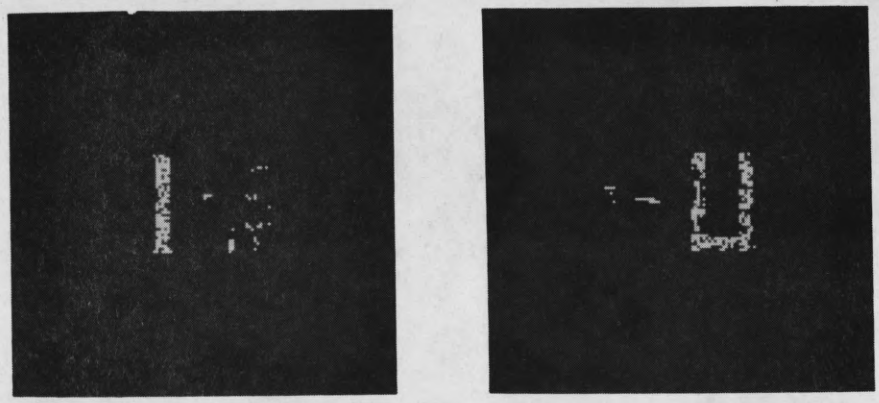

(a) (b)

Figure 5.11 (a) (b). Two Level Quantization in the Intensity of Figures 5.7 (a) (b). Intensity of Points I = 250 if I $\geq$ 150. (Scale 0 → 255)

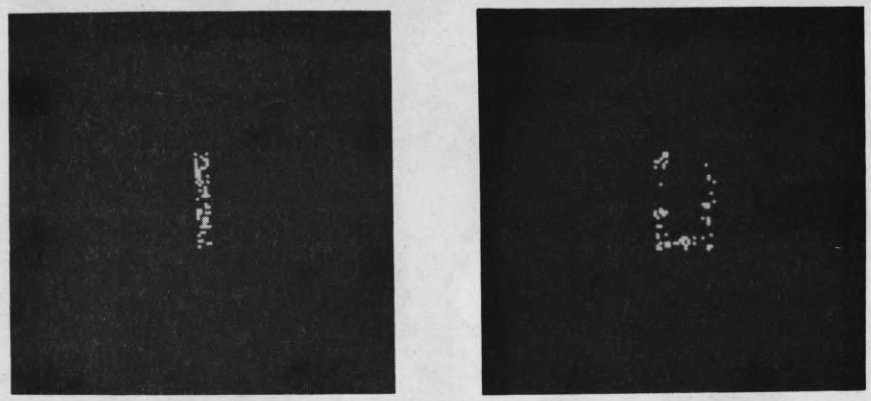

(a) (b)

Figures 5.12 (a) (b). Two Level Quantization in the Intensity of Figure 5.7 (a) (b). Intensity of Points I = 250 if I $\geq$ 100 (Scale 0 $\rightarrow$ 255).

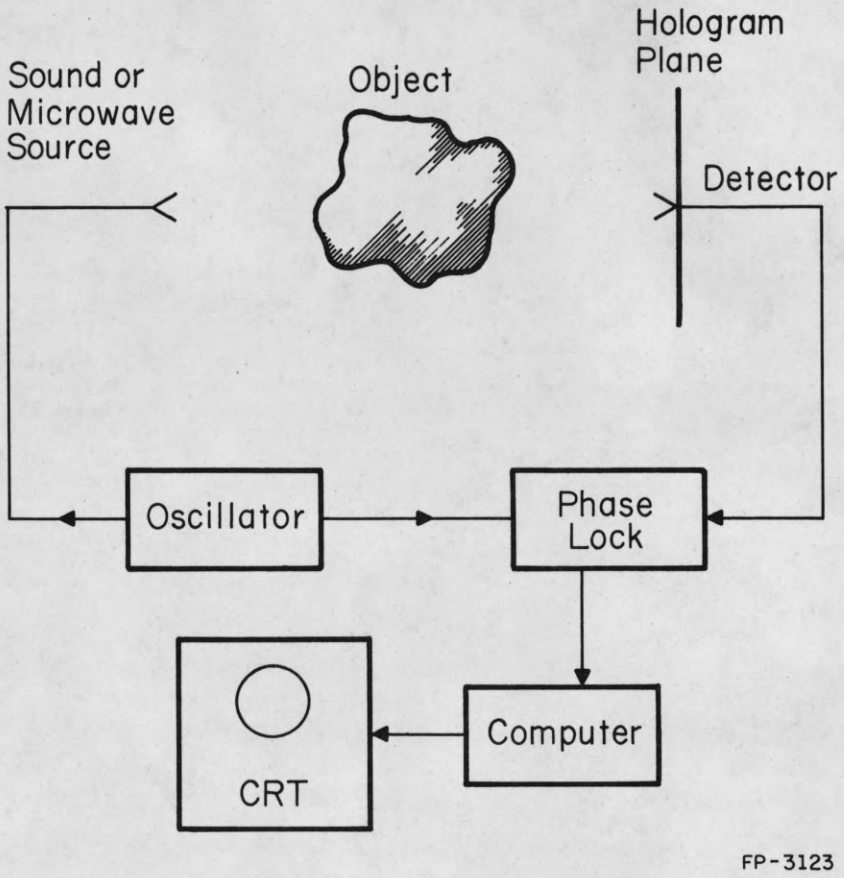

Figure 5.13 Almost Instant Display Arrangement for Image Reconstruction from Sound or Microwave Diffraction Field Patterns.

6. SUMMARY OF RESULTS AND CONCLUSIONS

6.1. Summary of Results

6.1.1. Synthetic Holograms

The method used to synthesize holograms of three-dimensional objects is analogous to the optical method of constructing holograms. In Chapter 2 a general theory of constructing holograms was presented and a technique for alleviating the longitudinal magnification inherent from the different recording and reconstructing wavelengths was presented. Experimental results described in Chapter 4 show that if the longitudinal dimension of the object is reduced in the recording process the longitudinal distortion of the final image is also reduced. The large depth of focus prohibits the complete elimination of the longitudinal distortion. Figures 4.3 (a), (b) indicate cross sections of optically reconstructed images. The depth of focus was evaluated and compared with the depth of the object. The depth of focus is the main disadvantage of the reported technique and it is inherent to three dimensional imaging using different recording and viewing wavelengths. The larger the depth of the object, the greater the reduction ratio m' possible and the less the resulting longitudinal distortion.

6.1.2. Image Reconstruction from Acoustic or Microwave Diffraction Patterns

In Chapter 5 a computer simulation for the reconstruction of images from simulated acoustic or microwave patterns is described. The digital reconstructions are applied in an attempt to gain some knowledge about the scattering object because as it was pointed out in Chapter 4 the optical reconstruction has certain limitations. Figures 5.4 (a), (b) show cross

sections of a digitally reconstructed image. The object illumination was nondiffuse and thus no speckle pattern appeared. Figure 5.7 (a), (b) indicate the case of image reconstruction from a diffusely illuminating object. More information about the object can be obtained by further processing the image, such as quantizing the levels of intensity.

6.2. Conclusions

In this investigation our aim has been to reconstruct images of objects from diffraction patterns recorded at sub-optical frequencies. Two methods for such a reconstruction were applied: optical and digital. For the optical reconstruction method, a technique for reducing the longitudinal distortion of the image in synthetic holograms is introduced. This allows one to partially reduce the longitudinal distortion but not completely due to the large depth of focus present. However, it is an improvement over the case where the technique is not applied. A disadvantage of the optical reconstruction method is that it yields a very small image. Larger apertures, more sampling points, along with improvements of the displaying system in the recording of holograms should greatly enhance the optical reconstruction technique.

The digital reconstruction method has the advantage over the optical, that it is simpler, faster, and gives larger images although not three dimensional ones. By displaying many cross sections of the reconstructed image, and picture processing of such sections, much information can be extracted from the cross sections to produce a three-dimensional perspective

of the object. Advances in computer technology will enhance more and more the digital reconstruction method. It is likely that digital reconstruction will become the dominant method of reconstructing images from sub-optical diffraction patterns.

REFERENCES

1. H. C. Andrews, Computer Techniques in Image Processing, Academic Press, New York, 1970.

2. Y. Aoki, "Acoustical Holograms and Optical Reconstruction," in Acoustical Holography (A. F. Metherell, H. M. A. El-Sum, and L. Larmore eds.) Vol. I, pp. 223-247, Plenum Press, New York, 1967.

3. Y. Aoki, "Optical and Numerical Reconstruction of Images from Sound-Wave Holograms," IEEE Trans. on Audio and Electroacoustics, Vol. AU-18, No. 3, pp. 258-267, September 1970.

4. G. D. Bergland, "A Guided Tour of the Fast Fourier Transform," IEEE Spectrum, pp. 41-52, July 1969.

5. M. Born and E. Wolf, Principles of Optics, Pergamonn Press, New York, 4th ed., 1970.

6. A. L. Boyer, J. A. Jordan, D. L. Van Rooy, P. M. Hirsch and L. B. Lesem, "Computer Reconstruction of Images from Ultrasonic Holograms," in Acoustical Holography (A. F. Metherell, and L. Larmore, eds.) Vol. II, pp. 211-223, Plenum Press, New York, 1970.

7. W. T. Cathey, Jr., "The Effects of Finite Sampling in Holography," Optik, Vol. 27, pp. 317-326, 1968.

8. W. T. Cochran and J. W. Cooley, et al., "What is the Fast Fourier Transform," Proc. of IEEE, Vol. 55, pp. 1664-1674, July 1967.

9. R. J. Collier, C. B. Burckhardt and L. H. Lin, Optical Holography, Academic Press, New York, 1971.

10. J. W. Cooley and J. W. Tukey, "An Algorithm for the Machine Calculation of Complex Fourier Series," Math. Comput., Vol. 19, pp. 297-301, April 1965.

11. G. A. Deschamps, "Some Remarks on Radio-Frequency Holography," Proc. IEEE, Vol. 55, p. 570, April 1967.

12. J. B. DeVelis and G. O. Reynolds, Theory and Applications of Holography, Addison-Wesley, Reading, Mass., 1967.

13. L. H. Enloe, "Noise-Like Structure in the Image of Diffusely Reflecting Objects in Coherent Illumination," Bell Syst. Tech. Journal, Vol. 46, pp. 1479-1489, 1967.

14. E. J. Feleppa, "Holography and Medicine," IEEE Proc. on Biomedical Eng., Vol. BME-19, pp. 194-205, May (1972).

15. D. Gabor, "Microscopy by Reconstructed Wave-Fronts," Proc. Roy. Soc. (London) A, Vol. 197, pp. 454-487, July 1949.

16. D. Gabor, "Microscopy by Reconstructed Wave-Fronts: II," Proc. Roy. Soc. (London) B, Vol. 64, pp. 449-469, June 1951.

17. D. Gabor, "Laser Speckle and its Elimination," IBM J. Res. Develop., Vol. 14, pp. 509-514, September 1970.

18. W. W. Gentleman and G. Sande, "Fast Fourier Transforms for Fun and Profit," 1966 Fall Joint Computer Conf., AFIPS Proc. Vol. 29, Washington, D.C.: Spartan 1966, pp. 563-578.

19. J. W. Goodman, Introduction to Fourier Optics, McGraw-Hill, New York, 1968.

20. J. W. Goodman, "Digital Image Formation from Detected Holographic Data," in Acoustical Holography, (A. F. Metherell, H. M. A. El-Sum, and L. Larmore, eds.) Vol. I, pp.173-185, Plenum Press, New York, 1969.

21. T. S. Huang, "Digital Holography," Proc. IEEE, Vol. 59, pp. 1335-1346, September 1971.

22. T. S. Huang, W. F. Schreiber and O. J. Tretiak, "Image Processing," Proc. IEEE, Vol. 59, pp. 1586-1609, November 1971.

23. Y. Ichioka, M. Izumi and T. Suzuki, "Scanning Halftone Plotter and Computer-Generated Continuous-Tone Hologram," Appl. Optics, 10, pp. 403-411, February 1971.

24. W. Kock, "Acoustics and Optics," Appl. Optics, Vol. 8, pp. 1525-1531, August 1969.

25. A. Korpel, "Acoustic Imaging and Holography," IEEE Spectrum, Vol. 5, pp. 45, 52, October 1968.

26. A. Kozma and D. L. Kelley, "Spatial Filtering for Detection of Signals Submerged in Noise," Appl. Optics, 4, pp. 387-392, April 1965.

27. E. Lalor, "Inverse Wave Propagator," J. Math Physics, Vol. 9, pp. 2001-2006.

28. W. H. Lee, "Sampled Fourier Transform Hologram Generated by Computer," Appl. Opt. 9, pp. 639-643, March 1970.

29. E. N. Leith and J. Upantnieks, "Reconstructed Wavefronts and Communication Theory," J. Opt. Soc. Am., Vol. 52, pp. 1123-1130, October 1962.

30. E. N. Leith and J. Upatnieks, Wavefront Reconstruction with Continuous-Tone Objects," J. Opt. Soc. Am., Vol. 53, pp. 1377-1381, December 1963.

31. E. N. Leith and J. Upatnieks, "Wavefront Reconstruction with Diffused Illumination and Three-Dimensional Objects," J. Opt. Soc. Am., Vol. 54, pp. 1295-1301, November 1964.

32. L. B. Lesem, P. M. Hirsch and J. A. Jordan, Jr., "Computer Generation and Reconstruction of Holograms," Proc. Symposium on Modern Optics, New York; Polytechnic Institute of Brooklyn, pp. 681-690, 1967.

33. L. B. Lesem, P. M. Hirsch and J. A. Jordan, "Computer Synthesis of Holograms for 3-D Display," Comm. Assoc. Comp. Machinery 12, pp. 661-674 (1968).

34. L. B. Lesem, P. M. Hirsch and J. A. Jordan, Jr., "The Kinoform: A New Wavefront Reconstruction Device," IBM J. Res. Develop. 13, pp. 150-155, March (1969).

35. A. P. Lohmann and D. P. Paris, "Binary Fraunhofer Holograms, Generated by Computer," Appl. Optics, 6, pp. 1739-1748, October 1967.

36. A. W. Lohmann and D. P. Paris, "Computer Generated Spatial Filters for Coherent Optical Data Processing," Appl. Optics. 7, pp. 651-655, April 1968.

37. R. S. Longhurst, Geometrical and Physical Optics, Longman, London, 1967.

38. A. J. MacGovern and J. C. Wyant, "Computer Generated Holograms for Testing Optical Elements," Appl. Optics, 10, pp. 619-624, March 1971.

39. R. Meier, "Magnification and Third-Order Aberrations in Holography," J. Opt. Soc. Am., Vol. 55, pp. 987-992, August 1965.

40. A. F. Metherell, H. M. A. El-Sum, J. J. Dreher and L. Larmore, "Introduction to Acoustical Holography," J. Acoust. Soc. Am., Vol. 42, pp. 733-742, April 1967.

41. R. Mittra and P. L. Ransom, "Imaging with Coherent Fields," Proc. Symposium on Modern Optics, New York: Polytechnic Institute of Brooklyn, 1967, pp. 619-647.

42. R. K. Mueller, E. Marom and D. Fritzler, "Some Problems Associated with Optical Image Formation from Acoustic Holograms," Appl. Optics, Vol. 8, pp. 1537-1542, August 1969.

43. R. K. Mueller, "Acoustic Holography," Proc. IEEE, Vol. 59, pp. 1319-1335, September 1971.

44. E. L. O'Neill, Introduction to Statistical Optics, Addison Wesley, Reading, Mass., 1963.

45. P. Papoulis, The Fourier Integral and its Applications, McGraw-Hill, New York, 1962.

46. K. Preston, Jr. and J. L. Kreuzer, " Ultrasonic Imaging Using a Synthetic Holographic Technique," Appl. Phys. Letters 10, pp. 150-152, March 1967.

47. P. L. Ransom, The Diffraction Transformation of Electromagnetic Fields Between Two Parallel Planes, Ph.D. Thesis, University of Illinois, Urbana, 1969.

48. J. R. Shewell and E. Wolf, "Inverse Diffraction and a New Reciprocity Theorem," J. of Optical Soc. of America, Vol. 58, pp. 1596-1603, December 1968.

49. H. M. Smith, Principles of Holography, Wiley-Intersciences, New York, 1969.

50. M. M. Sondhi, "Reconstruction of Objects from Their Sound-Diffraction Patterns," J. Acoustical Society of America, Vol. 46, Pt. 2, pp. 1158-1164, April 1969.

51. T. G. Stockham, Jr., "High-Speed Convolution and Correlation," 1966 Spring Joint Computer Conf., AFIPS Proc., Vol. 18, Washington D. C.: Spartan, 1966, pp. 229-233.

52. G. W. Stroke, An Introduction to Coherent Optics and Holography, Academic Press, New York, 1969.

53. A. Vander Lugt, "A Review of Optical Data-Processing Techniques," Optica Acta, Vol. 15, pp. 1-33, 1968.

54. J. P. Walters, "Holographic Image Synthesis Utilizing Theoretical Methods," Appl. Physics Letters, Vol. 9, pp. 405-407, December 1966.

Security Classification

DOCUMENT CONTROL DATA - R & D

(Security classification of title, body of abstract and indexing annotation must be entered when the overall report is classified)

1. ORIGINATING ACTIVITY *(Corporate author)*

Coordinated Science Laboratory
University of Illinois
Urbana, Illinois 61801

2a. REPORT SECURITY CLASSIFICATION

UNCLASSIFIED

2b. GROUP

3. REPORT TITLE

SYNTHETIC HOLOGRAMS AND IMAGE RECONSTRUCTION FROM ACOUSTIC OR MICROWAVE FIELD PATTERNS

4. DESCRIPTIVE NOTES *(Type of report and inclusive dates)*

5. AUTHOR(S) *(First name, middle initial, last name)*

Themistocles H. Demetrakopoulos and Raj Mittra

6. REPORT DATE	7a. TOTAL NO. OF PAGES	7b. NO. OF REFS
October, 1972	72	54

8a. CONTRACT OR GRANT NO.	9a. ORIGINATOR'S REPORT NUMBER(S)
DAAB-07-67-C-0199;	
b. PROJECT NO. Army Research Grant G-77	R-591
c.	9b. OTHER REPORT NO(S) *(Any other numbers that may be assigned this report)*
d.	UILU-ENG 72-2253

10. DISTRIBUTION STATEMENT

This document has been approved for public release and sale; its distribution is unlimited.

11. SUPPLEMENTARY NOTES	12. SPONSORING MILITARY ACTIVITY
	Joint Services Electronics Program through U. S. Army Electronics Command, Fort Monmouth; Army Research Office

13. ABSTRACT

Recently there has been much interest in the area of acoustic or microwave holography since the use of these sources allow one to image through some optically opaque media.

Optical reconstruction applied to holograms that have been recorded at microwave, acoustic or other sub-optical frequencies produced a longitudinally distorted image, unless the original hologram has been reduced by the ratio of the recording to reconstructing wavelength. Since the required reduction ratio is very large it is difficult to achieve it in practice. Also, a hologram reduced in this manner reproduces an image that is extemely small. In this investigation a technique is presented for the reduction, or complete elimination, of the longitudinal distortion in three-dimensional imaging from synthetic holograms. The object is longitudinally demagnified in the recording process, an optical hologram is synthesized and subsequently reduced by a suitable factor. Next, the image is reconstructed by illuminating the hologram with laser light. Due to the difference of the recording and reconstructing wavelengths the image is longitudinally distorted. However, in principle the longitudinal demagnification introduced in the recording process can be made to compensate, either totally or in part, the longitudinal magnification introduced in the reconstruction process. In practice the large depth of focus inherent from the small ratio of the hologram aperture to wavelength limits the use of this technique to partial compensation only.

DD FORM 1 NOV 65 1473

Security Classification

14 KEY WORDS	LINK A		LINK B		LINK C	
	ROLE	WT	ROLE	WT	ROLE	WT
Holography						
Diffraction						
Acoustical holography						
Computer-generated holograms						